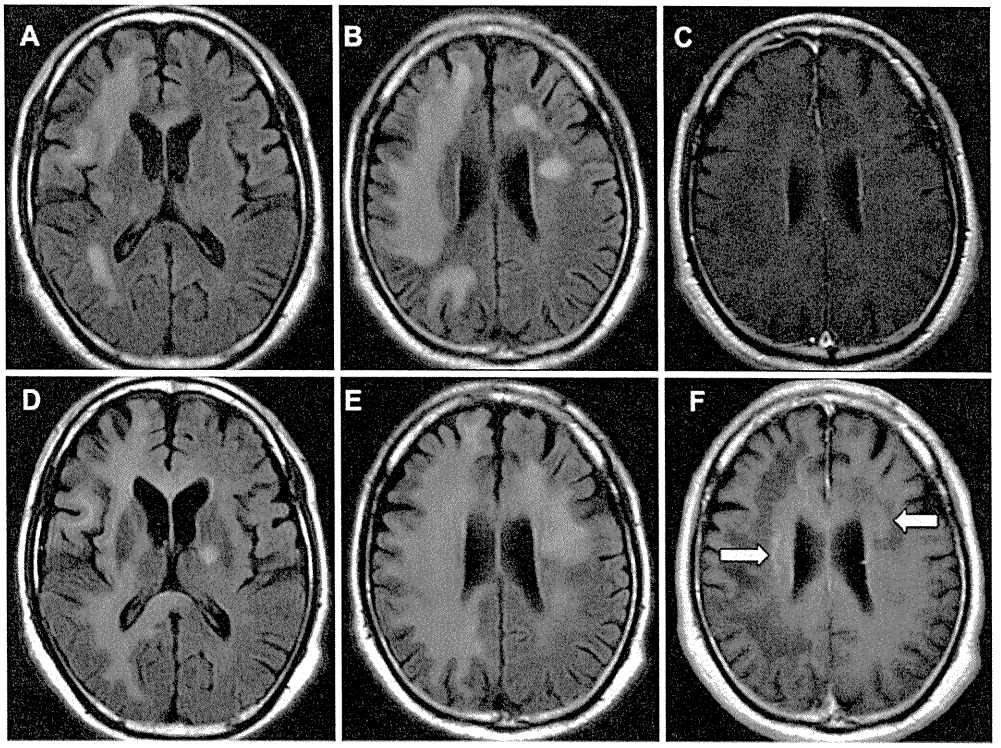

Figure 1. **A, B and C show the initial MR study at admission (3 months after onset). A fluid attenuation inversion recovery (FLAIR) image showed hyperintense signals in the bilateral fronto-parietal white matter (A, B). A T1-weighted post-gadolinium contrast image showed no enhancement (C). D, E and F show the follow-up MR study 8 months after onset (5 weeks after initiation of mefloquine). A FLAIR image showed progression of white matter abnormalities (D, E). A T1-weighted post-gadolinium contrast image showed diffuse enhancement of white matter abnormalities (arrows) (F).**

Case Report

A 55-year-old man presented with memory impairment and communication disorder in January 2010. His cognitive dysfunction worsened, and he was admitted to our hospital in mid-March. Clinical examination revealed attention disturbance, left hemispatial neglect, apraxia, memory impairment and dysarthria. The patient did not show any signs of paralysis or involuntary movement, and muscle tonus and tendon reflexes were normal. The white blood cell count was 4.58×10^3/μL (CD4+ lymphocyte: 187/μL, CD8+ lymphocyte: 1,070/μL), HIV antibodies were positive, and HIV RNA was 50.0×10^3 copies/mL in his blood. An examination of the cerebrospinal fluid (CSF) showed increased protein concentration (88 mg/dL) and a normal cell count (2/μL with all mononuclear cells), and real-time polymerase chain reaction (PCR) for JCV DNA in the CSF yielded positive results, showing 535,500 copies/mL. On admission MRI (Signa Excite HD 3.0 T: GE Medical Systems) showed T2 and fluid attenuated inversion recovery (FLAIR) asymmetrical high signals in the cerebral bilateral white matter, and the cortex was almost completely intact although the lesion involved the U-fibers. DWI (*b*-value, 1,000 s/mm^2) showed high signals in the part of hyperintense lesion on T2WI/FLAIR. MR imaging did not show any gadolinium enhancement (Fig. 1A, B, C). MRS using the GE technique PROBE with PRESS; TR 2,000 ms; TE 144 ms was performed, as well. The ^{1}H-MR spectrum was acquired from a localized voxel of interest outlined in an axial FLAIR image of the right frontal periventricular white matter lesion. The voxel size was 20×20×20 mm (volume, 8 cm^3). ^{1}H-MRS showed a substantially reduced N-acetylaspartate (NAA)/creatine (Cr) ratio (NAA/Cr=0.57) and an elevated choline (Cho)/creatine ratio (Cho/Cr=1.76) (Fig. 2A, B). On the apparent diffusion coefficient map (ADC map), ADC values were measured in five regions of interest in the right frontal periventricular white matter lesion, and the values were found to increase slightly (range 0.84 to 1.04, mean value 0.94×10^{-3} mm^2/s) (Fig. 2C, D). Probable PML associated with HIV infection was diagnosed.

HAART was initiated in April 2010, four months after the onset of symptoms. Following treatment, the HIV-RNA level decreased, but CD4+ lymphocytes were under 200/μL throughout the course and did not show substantial elevation. The MRI findings and clinical manifestations deteriorated, and the patient developed left flaccid hemiplegia and experienced akinetic mutism. In June 2010, about six months after the onset, treatment with mefloquine hydrochloride tablets was started at 275 mg/day orally for three

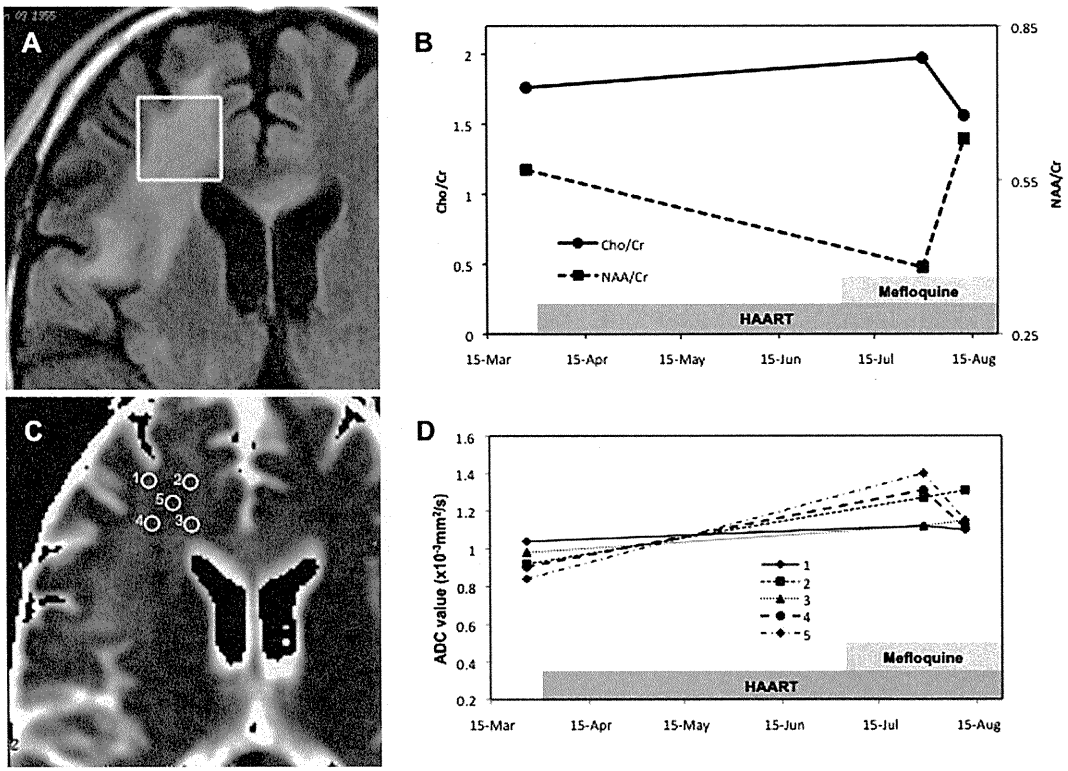

Figure 2. **^{1}H-MRS and DWI were performed on March 26, July 29 and August 11. A. ^{1}H-MR spectrum acquired from a localized voxel of interest outlined on an axial FLAIR image of the right frontal periventricular white matter lesion. B. Serial change of ^{1}H-MRS at three time points. The third ^{1}H-MRS (5 weeks after the initiation of mefloquine) showed an increased ratio of N-acetyl-aspartate (NAA) and a decreased ratio of choline (Cho) to creatine (Cr) with improvement of symptoms. C. The ADC value was measured in the apparent diffusion coefficient map (ADC map) in five regions of interest (i.e., 1-5) in the right frontal periventricular white matter lesion. D. Serial changes of the ADC value at three time points. ADC values showed a slight upward tendency, whereas some ADC values (i.e. 1,4,5) decreased at the third DWI study.**

days and was then continued at 275 mg once a week. This course followed the administration protocol of Kishida et al (7) as a modification of the Biogen Idec mefloquine treatment protocol taken from the clinicaltrials.gov website (8). According to the instructions of the ethical review board at Hiroshima University Hospital, informed consent regarding the use of mefloquine was obtained from the patient's family prior to introduction of the therapy. About eight months after the onset, and five weeks after mefloquine was started, the patient showed some improvement of clinical symptoms, and an MRI revealed enhancing white matter lesions (Fig. 1D, E, F). ^{1}H-MRS of the right frontal lesion showed a further reduction in NAA (NAA/Cr=0.38) and elevated Cho (Cho/Cr=1.97) (Fig. 2B). All ADC values showed an increasing trend, and the mean ADC value was 1.244×10^{-3} mm^2/s (range 1.12 to 1.40×10^{-3} mm^2/s) (Fig. 2D). The patient's clinical condition continued to improve, and he began to let out a single tone and showed improved muscle strength in his left arm and leg. ^{1}H-MRS performed seven weeks after mefloquine was introduced showed recoveries of reduced NAA (NAA/Cr=0.63) and elevated Cho (Cho/Cr= 1.56) in comparison to the levels at admission (Fig. 2B). Several ADC values showed a slight decreasing trend, and the mean ADC value was 1.164×10^{-3} mm^2/s (range 1.10 to 1.31×10^{-3} mm^2/s) (Fig. 2D). Eight weeks after mefloquine was introduced, CSF PCR findings for JCV were negative. In August 2010, the patient was transferred to another hospital.

Discussion

Compared with the era before combined anti-retroviral therapy, the incidence and mortality of HIV-PML are currently reduced; however, HIV-PML is still a fatal disease due to the treatment-resistant cases. Several factors are considered to be involved in HIV-PML prognosis including CD4+ T cell count. Marzocchetti et al (9) reported that the estimated 1-year survival rate was 48% in HIV-positive PML patients with a CD4 count <200/μL at PML diagnosis compared to 67% in those with a CD4 count >200/μL. In addition, JC viral load in the CSF can be attributed to long-term survival. In a study of 61 HIV-infected patients with PML, Bossolasco et al (10) reported that JCV DNA levels of >3.64 log copies/mL were significantly correlated with a shorter survival. And thus the reasons for the resistance to HAART in the present case may include low-CD4+ T cell

counts and high levels of JCV DNA during therapeutic period.

Recently, the anti-malarial drug mefloquine, which is considered to have anti-JCV action, is expected to have an effect on PML, and a randomized study is currently underway (8). Gofton et al (5) reported a patient with sarcoidosis who was treated with 1,000 mg/week mefloquine that was initiated six months after symptom onset. Clinical progression stopped immediately, and the JC virus then became undetectable in the CSF. Kishida and Tanaka (6) reported a patient after an umbilical cord blood transplant that showed favourable clinical, neuroradiological and virological responses after the initiation of mefloquine. To our knowledge, the present case is the first detailed report that demonstrates that mefloquine combined with HARRT gave a positive outcome to a patient with HIV-PML. Although mefloquine was initiated six months after symptom onset, the result implies that mefloquine has the ability to improve symptoms of HAART-resistant PML even in the chronic phase.

Image findings in PML reflect demyelination and provide helpful information for diagnosis. Contrast enhancement is usually absent in classic PML lesions on MRI because the lesions are oligodendrocyte cell death caused by persistent JCV infection, which indicates that the lesions are not associated with inflammation. It is possible that contrast enhancement in PML is caused by mechanisms of the inflammatory response induced when JCV is eliminated by the immune system. When this response causes massive cellular destruction after initiation of HAART, an HIV-PML patient's clinical condition sometimes becomes worse. This worsening is known as immune reconstitution inflammatory syndrome. However, once JCV is eliminated by the immune system, an improvement in the prognosis can be expected. There are reports that contrast enhancement is a favourable treatment response (11, 12) and associated with a longer survival (13-15). In the present case, the PML was advanced, because the CD4+ T cell count did not increase, and the immune system did not recover only by HAART. About five weeks after mefloquine was initiated, an MRI showed an enhancing lesion corresponding to symptomatic improvement. This MRI finding may imply an inflammatory response against JCV-infected cells in the lesion.

There have been some studies on white matter lesions using DWI. It has been shown that the ADC value in a recent lesion and an advancing edge of established lesion decreases, and the ADC value in an old lesion and in the center of the lesion increases (16-18). In the present case, as the clinical condition became worse, the elevated ADC value in the lesion showed a further increase in spite of HAART. In PML lesions, an increased ADC value indicates pathologically enlarged extracellular space and a loss of myelin (17). There are some reports of serial ADC value changes in PML patients treated with HAART (18, 19). Usiskin et al (18) reported an HIV-PML patient who presented a decreased ADC value with a favourable response to therapy, and they suggested that the change implied microstructural reorganization. In the present case, the ADC value also decreased slightly with an improvement in the clinical condition after the introduction of mefloquine. There is a possibility that facilitated diffusion becoming slightly more restricted shows remyelination in the white matter lesion.

Early ^{1}H-MRS studies of patients with PML have revealed that decreased NAA concentrations [which indicate neuronal damage (20)], elevated Cho (which indicates demyelination), and the appearance of a lactate peak (which indicates impaired energy metabolism) (21-23). In the present case, serial changes of ^{1}H-MRS were observed. ^{1}H-MRS performed seven weeks after mefloquine was introduced revealed elevated NAA/Cr and reduced Cho/Cr, reflecting an improvement in clinical symptoms. This change may indicate a functional improvement of infected oligodendrocytes by anti-JCV effects of mefloquine. Several studies have demonstrated that a decrease of NAA could be partially reversible in acute demyelinating lesions (such as those that occur in multiple sclerosis patients) (24-26).

There is a possibility that mefloquine is effective in the chronic phase of HAART-resistant cases of HIV-PML. The present results suggest that, in addition to contrast enhancement, DWI and ^{1}H-MRS may offer valuable information on the microstructural reorganization process that occurs after mefloquine inhibits oligodendrocyte death.

The authors state that they have no Conflict of Interest (COI).

Acknowledgement

The authors are grateful to Dr. Kazuo Nakamichi and Dr. Masayuki Saijo (Department of Virology 1, National Institute of Infectious Diseases) for determinations of JCV in CSF and Dr. Motohiro Yukitake (Division of Neurology, Department of Internal Medicine Faculty of Medicine, Saga University) for helpful suggestions on the use of mefloquine.

References

1. Molloy ES, Calabrese LH. Progressive multifocal leukoencephalopathy: a national estimate of frequency in systemic lupus erythematosus and other rheumatic diseases. Arthritis Rheum **60**: 3761-3765, 2009.
2. Antinori A, Cingolani A, Lorenzini P, et al. Italian Registry Investigative Neuro AIDS Study Group. Clinical epidemiology and survival of progressive multifocal leukoencephalopathy in the era of highly active antiretroviral therapy: data from the Italian Registry Investigative Neuro AIDS (IRINA). J Neurovirol **9**: 47-53, 2003.
3. Koralnik IJ. New insights into progressive multifocal leukoencephalopathy. Curr Opin Neurol **17**: 365-370, 2004.
4. Brickelmaier M, Lugovskoy A, Kartikeyan R, et al. Identification and characterization of mefloquine efficacy against JC virus in vitro. Antimicrob Agents Chemother **53**: 1840-1849, 2009.
5. Gofton TE, Al-Khotani A, O'Farrell B, Ang LC, McLachlan RS. Mefloquine in the treatment of progressive multifocal leukoencephalopathy. J Neurol Neurosurg Psychiatry **82**: 452-455, 2011.
6. Kishida S, Tanaka K. Mefloquine treatment in a patient suffering from progressive multifocal leukoencephalopathy after umbilical cord blood transplant. Intern Med **49**: 2509-2513, 2010.
7. Kishida S, Tanaka K, Ajisawa A, et al. Annual report of the re-

search committee on prion disease and slow virus infection, research on measures for intractable diseases health and labour sciences research grants, the Ministry of Health. Labour and Welfare of Japan, 2010: 125-132 (in Japanese).

8. Clinical Trials.gov [Internet]. Maryland: U.S. National Institutes of Health; c1993- [updated 2011 July 7; cited 2011 Jul 25]. Study to Explore the Effect of Mefloquine in Subjects with Progressive Multifocal Leukoencephalopathy (PML). Available from: http://clinicaltrials.gov/ct2/show/NCT00746941
9. Marzocchetti A, Tompkins T, Clifford DB, et al. Determinants of survival in progressive multifocal leukoencephalopathy. Neurology **73**: 1551-1558, 2009.
10. Bossolasco S, Calori G, Moretti F, et al. Prognostic significance of JC virus DNA levels in cerebrospinal fluid of patients with HIV-associated progressive multifocal leukoencephalopathy. Clin Infect Dis **40**: 738-744, 2005.
11. Thurnher MM, Post MJ, Rieger A, Kleibl-Popov C, Loewe C, Schindler E. Initial and follow-up MR imaging findings in AIDS-related progressive multifocal leukoencephalopathy treated with highly active antiretroviral therapy. AJNR Am J Neuroradiol **22**: 977-984, 2001.
12. Du Pasquier RA, Koralnik IJ. Inflammatory reaction in progressive multifocal leukoencephalopathy: harmful or beneficial? J Neurovirol **9**: 25-31, 2003.
13. Berger JR, Levy RM, Flomenhoft D, Dobbs M. Predictive factors for prolonged survival in acquired immunodeficiency syndrome-associated progressive multifocal leukoencephalopathy. Ann Neurol **44**: 341-349, 1998.
14. Arbusow V, Strupp M, Pfister HW, Seelos KC, Brückmann H, Brandt T. Contrast enhancement in progressive multifocal leukoencephalopathy: a predictive factor for long-term survival? J Neurol **247**: 306-308, 2000.
15. Küker W, Mader I, Nägele T, et al. Progressive multifocal leukoencephalopathy: value of diffusion-weighted and contrast-enhanced magnetic resonance imaging for diagnosis and treatment control. Eur J Neurol **13**: 819-826, 2006.
16. Mader I, Herrlinger U, Klose U, Schmidt F, Küker W. Progressive multifocal leukoencephalopathy: analysis of lesion development with diffusion-weighted MRI. Neuroradiology **45**: 717-721, 2003.
17. Bergui M, Bradac GB, Oguz KK, et al. Progressive multifocal leukoencephalopathy: diffusion-weighted imaging and pathological correlations. Neuroradiology **46**: 22-25, 2004.
18. Usiskin SI, Bainbridge A, Miller RF, Jäger HR. Progressive multifocal leukoencephalopathy: serial high-b-value diffusion-weighted MR imaging and apparent diffusion coefficient measurements to assess response to highly active antiretroviral therapy. AJNR Am J Neuroradiol **28**: 285-286, 2007.
19. Buckle C, Castillo M. Use of diffusion-weighted imaging to evaluate the initial response of progressive multifocal leukoencephalopathy to highly active antiretroviral therapy: early experience. AJNR Am J Neuroradiol **31**: 1031-1035, 2010.
20. Nakano M, Ueda H, Li JY, Matsumoto M, Yanagihara T. Measurement of regional N-acetylaspartate after transient global ischemia in gerbils with and without ischemic tolerance: an index of neuronal survival. Ann Neurol **44**: 334-340, 1998.
21. Iranzo A, Moreno A, Pujol J, et al. Proton magnetic resonance spectroscopy pattern of progressive multifocal leukoencephalopathy in AIDS. J Neurol Neurosurg Psychiatry **66**: 520-523, 1999.
22. Chang L, Ernst T, Tornatore C, et al. Metabolite abnormalities in progressive multifocal leukoencephalopathy by proton magnetic resonance spectroscopy. Neurology **48**: 836-845, 1997.
23. Cuvinciuc V, Martin-Blondel G, Marchou B, et al. Proton MR Spectroscopy of progressive multifocal leukoencephalopathy-immune reconstitution inflammatory syndrome. Am J Neuroradiol **31**: 69-70, 2010.
24. Narayanan S, De Stefano N, Francis GS, et al. Axonal metabolic recovery in multiple sclerosis patients treated with interferon beta-1b. J Neurol **248**: 979-986, 2001.
25. Matsui N, Nakane S, Harada M, et al. Neuroradiological study of a possible progressive multifocal leukoencephalopathy using diffusion tensor imaging and proton magnetic resonance spectroscopy. Rinsho Shinkeigaku (Clin Neurol) **46**: 555-560, 2006 (in Japanese, Abstract in English).
26. Dreha-Kulaczewski SF, Helms G, Dechent P, Hofer S, Gärtner J, Frahm J. Serial proton MR spectroscopy and diffusion tensor imaging in infantile Balo's concentric sclerosis. Neuroradiology **51**: 113-121, 2009.

© 2012 The Japanese Society of Internal Medicine
http://www.naika.or.jp/imindex.html

OPEN ACCESS Freely available online

PLoS one

Granulovacuolar Degenerations Appear in Relation to Hippocampal Phosphorylated Tau Accumulation in Various Neurodegenerative Disorders

Yuu Yamazaki[1]*, Tomoyasu Matsubara[2], Tetsuya Takahashi[1], Takashi Kurashige[1], Eisuke Dohi[1], Masanori Hiji[1,3], Yoshito Nagano[1], Takemori Yamawaki[1], Masayasu Matsumoto[1]

1 Department of Clinical Neuroscience and Therapeutics, Hiroshima University Graduate School of Biomedical Sciences, Hiroshima, Japan, **2** Department of General Internal Medicine, Aso Iizuka Hospital, Iizuka, Japan, **3** Department of Neurology, Mifukai Viha-ra Hananosato Hospital, Miyoshi, Japan

Abstract

Background: Granulovacuolar degeneration (GVD) is one of the pathological hallmarks of Alzheimer's disease (AD), and it is defined as electron-dense granules within double membrane-bound cytoplasmic vacuoles. Several lines of evidence have suggested that GVDs appear within hippocampal pyramidal neurons in AD when phosphorylated tau begins to aggregate into early-stage neurofibrillary tangles. The aim of this study is to investigate the association of GVDs with phosphorylated tau pathology to determine whether GVDs and phosphorylated tau coexist among different non-AD neurodegenerative disorders.

Methods: An autopsied series of 28 patients with a variety of neurodegenerative disorders and 9 control patients were evaluated. Standard histological stains along with immunohistochemistry using protein markers for GVD and confocal microscopy were utilized.

Results: The number of neurons with GVDs significantly increased with the level of phosphorylated tau accumulation in the hippocampal regions in non-AD neurodegenerative disorders. At the cellular level, diffuse staining for phosphorylated tau was detected in neurons with GVDs.

Conclusions: Our data suggest that GVDs appear in relation to hippocampal phosphorylated tau accumulation in various neurodegenerative disorders, while the presence of phosphorylated tau in GVD-harbouring neurons in non-AD neurodegenerative disorders was indistinguishable from age-related accumulation of phosphorylated tau. Although GVDs in non-AD neurodegenerative disorders have not been studied thoroughly, our results suggest that they are not incidental findings, but rather they appear in relation to phosphorylated tau accumulation, further highlighting the role of GVD in the process of phosphorylated tau accumulation.

Citation: Yamazaki Y, Matsubara T, Takahashi T, Kurashige T, Dohi E, et al. (2011) Granulovacuolar Degenerations Appear in Relation to Hippocampal Phosphorylated Tau Accumulation in Various Neurodegenerative Disorders. PLoS ONE 6(11): e26996. doi:10.1371/journal.pone.0026996

Editor: John Duda, Philadelphia VA Medical Center, United States of America

Received September 1, 2011; **Accepted** October 7, 2011; **Published** November 3, 2011

Copyright: © 2011 Yamazaki et al. This is an open-access article distributed under the terms of the Creative Commons Attribution License, which permits unrestricted use, distribution, and reproduction in any medium, provided the original author and source are credited.

Funding: This work was supported by the Ministry of Education, Culture, Sports, Science and Technology (MEXT: http://www.mext.go.jp/english/) and Grant-in-Aid for Scientific Research (C) (#21591085; Principle Investigator, Tetsuya Takahashi). The funders had no role in study design, data collection and analysis, decision to publish, or preparation of the manuscript.

Competing Interests: The authors have declared that no competing interests exist.

* E-mail: yyamazak@hiroshima-u.ac.jp

Introduction

Granulovacuolar degeneration (GVD) is one of the pathological hallmarks of Alzheimer's disease (AD) [1] and is defined as electron-dense granules within double membrane-bound cytoplasmic vacuoles, mainly in the hippocampal pyramidal neurons [2].

Attempts to define the molecular composition of GVDs by immunohistochemical methods led to the identification of a large number of possible protein constituents, suggesting a link between GVD and AD-related neurodegeneration. For example, the tau protein found in GVD complexes is antigenically related to that found in paired helical filaments in AD, although antibodies to other forms of tau do not recognize GVDs [3,4,5,6]. Activation of caspase 3, an apoptotic effector protease involved in cleavage of tau [7] and amyloid precursor protein [8], has been found in GVDs, but rarely in other pathological structures [9,10,11,12]. The protein kinases glycogen-synthase kinase 3 and casein kinase 1, which phosphorylate tau, are also markers of GVD [13,14,15,16,17]. Phosphorylated pancreatic endoplasmic reticulum kinase, a marker of a cellular stress response to unfolded protein, which is increased in AD, is associated with GVD [18]. Intraneuronal dot-like structures morphologically similar to GVDs were also labelled by phosphorylation-dependent TAR DNA binding protein (TDP43) antibody [19], in line with the abnormal TDP43 immunoreactivity reported in AD [20,21,22,23,24,25]. Furthermore, both proteasome and endosome pathway dysfunction may be present in GVD-containing cells, as GVD has been detected by antibodies to a cellular marker of proteasome degradation, ubiquitin (Ub) [2,26], to intermediaries in the ubiquitin system, phospho-β-catenin [27] and Pin1 [28], and to

the endosome-related protein charged multivesicular body protein 2b (CHMP2B) [29,30]. In relation to other pathognomonic features, several lines of evidence have suggested that GVDs appear within the hippocampal pyramidal neurons in AD when phosphorylated tau begins to aggregate into early-stage neurofibrillary tangles (NFTs) [11,15,18,31].

However, GVDs are not AD-specific hallmark: they have been reported within the hippocampal pyramidal neurons in normal aged brain [32], as well as in other diseases such as progressive supranuclear palsy (PSP) [33], pantothenate kinase-associated neurodegeneration (PKAN) [34], corticobasal degeneration (CBD) [35] and Pick's disease (PiD) [36]. Given that all these disorders can present with pathological lesions containing phosphorylated tau protein, these findings raise the possibility that GVDs may also appear in relation to the hippocampal phosphorylated tau accumulation in non-AD neurodegenerative disorders.

Recently, we have shown that an antibody to CHMP2B can specifically detect GVDs within hippocampal pyramidal neurons in AD [29]. The high sensitivity and specificity of this antibody were later confirmed by another group [30]. CHMP2B is a component of the endosomal sorting complex required for transport III (ESCRT-III), which is involved in endocytic trafficking of proteins [37]. ESCRT-III drives the formation and specifically the scission of intraluminal vesicles in multivesicular bodies, and under certain conditions remains associated with them.

To better understand GVD formation, particularly focusing on its relationship with the accumulation of phosphorylated tau, we examined GVDs in non-AD neurodegenerative disorders. The aims of the present study were: (1) to compare the CHMP2B immunopositivity of the hippocampal GVDs in several neurodegenerative disorders that can present with pathological lesions containing phosphorylated tau protein; and (2) to investigate the association of CHMP2B-positive GVDs with tau pathology, to determine whether CHMP2B-positive GVDs and phosphorylated tau coexist among non-AD neurodegenerative disorders.

Results

CHMP2B-positive granules correspond to GVDs in the hippocampal neurons from patients with several neurodegenerative disorders

Immunohistochemical localization of CHMP2B was investigated in the hippocampus of several neurodegenerative disorders, including MyD, ALS-D, PDD, MSA, PiD, PSP and PKAN cases. As reported, CHMP2B immunoreactivity was observed as granules in pyramidal neurons. No immunoreactivity was detected in glial cells. CHMP2B-positive granules were often surrounded by a clear halo and were morphologically similar to the classic granules of GVD.

To confirm the GVD nature of these CHMP2B-positive granules, sections were stained once with hematoxylin and eosin (Fig. 1A, B, E, F, I, J). After observing GVDs in the hippocampus, these stained sections were de-stained in absolute ethanol, and processed for CHMP2B immunohistochemical analysis (Fig. 1C, D, G, H, K, L). Most neurons with GVDs showed CHMP2B-positive granules and these CHMP2B-positive granules corresponded to GVDs. Together with our previous results, this suggested that CHMP2B could be used as a molecular label to study GVD in non-AD neurodegenerative disorders. The numbers of neurons with CHMP2B-positive GVDs/mm^2 in each case are listed in Table S1.

CHMP2B-positive GVDs colocalize with pSmad2/3 and ubiquitin

Since GVDs have been reported to be immunoreactive for pSmad2/3 [38] and Ub [2,26], we assessed the colocalization of CHMP2B-positive GVDs and these markers using double immunofluorescent labeling. In the hippocampus of several neurodegenerative disorders, including MyD, ALS-D, PDD, MSA, and PKAN cases, almost all CHMP2B-positive GVDs were also immunopositive for pSmad2/3 and Ub (Fig. 2). The colocalization of CHMP2B-positive GVDs and these markers could also be observed even in PSP (Fig. 2J, K, L, JJ, KK, LL) and MSA-C cases (Fig. 2G, H, I, GG, HH, II), in which hematoxylin and eosin staining revealed relatively few GVDs that we could not confirm the GVD nature of CHMP2B-positive granules.

To investigate the reliability of using CHMP2B as a molecular label to study GVDs, we next examined the correlation between the number of neurons with CHMP2B-positive GVDs and the number of neurons with granules immunopositive for pSmad2/3 or Ub. As shown in Figure 3A, immunohistochemistry with the anti-CHMP2B antibody detected GVDs in a similar number of cells to those immunoreactive for pSmad2/3 or Ub within the hippocampal region in each of the diseases studied.

CHMP2B-positive GVDs correlate with hippocampal tau pathology phosphorylated at Ser-202 and Thr-205

Our research interest was the association of CHMP2B-positive GVDs with tau pathology in the hippocampus, including the subiculum, CA2 and CA1 subfields, where GVDs were found in high number in AD as well as non-AD cases [18,39]. Therefore we directly compared the number of hippocampal neurons with CHMP2B-positive GVDs with the number of neurons positive for phosphorylated tau. The number of neurons positive for phosphorylated tau was assessed using our method for scoring tangle densities (for details see the Material and Methods). We also investigated the association between neurons with CHMP2B-positive GVDs and classic Braak NFT stage. The phosphorylated tau score (p-tau score) and Braak stage score in each case are listed in Table 1, right column.

When age at death was controlled, strong correlations were observed between both the number of neurons with CHMP2B-positive GVDs and p-tau score ($r = 0.63$, $p < 0.01$) as well as CHMP2B-positve GVDs and Braak NFT stage ($r = 0.77$, $p < 0.01$) across the entire sample. Strong correlations were also observed when we excluded AD cases from the analysis ($r = 0.60$, $p < 0.01$, Fig. 3B, $r = 0.73$, $p < 0.01$, Fig. 3C, respectively).

We next investigated the correlation between CHMP2B-positive GVDs and phosphorylated tau at the cellular level. For immunohistochemistry, we used the AT8 antibody, which recognizes tau phosphorylated at Ser-202 and Thr-205. In addition to NFTs, in AD and other neurodegenerative diseases AT8 stains some non-tangle-bearing pyramidal neurons, indicative of hyperphosphorylated tau in a pre-tangle stage [40]. While no or very few CHMP2B-positive GVDs were observed in neurons with NFTs immunoreactive for AT8, diffuse staining for phosphorylated tau was observed in neurons with CHMP2B-positive GVDs in several neurodegenerative disorders, except for the cases in which immunohistochemistry revealed relatively few CHMP2B-immunoreactive neurons (Table S1 and Fig. 4). Together, these data indicate that CHMP2B-positive GVDs appear in association with the accumulation of phosphorylated tau in several neurodegenerative disorders.

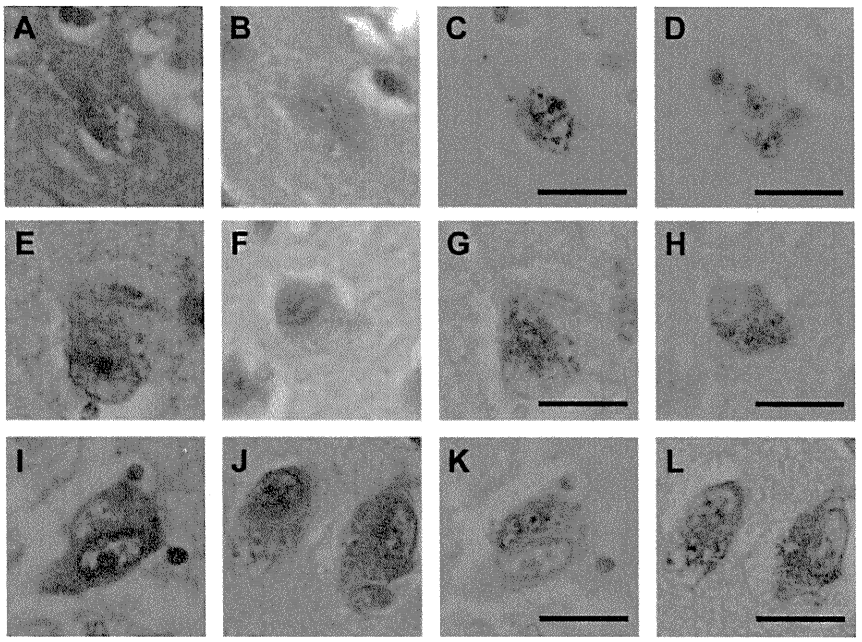

Figure 1. CHMP2B-positive granules correspond to GVDs. Cellular localization of CHMP2B (**C, D, G, H, K, L**) compared with hematoxylin and eosin (HE) staining (**A, B, E, F, I, J**) in several neurodegenerative disorders is shown. CHMP2B-positive structures colocalized with the GVDs identified by HE staining and surrounded by a clear halo. **A, C**, Alzheimer's disease; **B, D**, myotonic dystrophy; **E, G**, amyotrophic lateral sclerosis with dementia; **F, H**, Pick's disease; **I, K**, multiple system atrophy with parkinsonism; **J, L**, pantothenate kinase-associated neurodegeneration. Scale bars represent 20 μm.
doi:10.1371/journal.pone.0026996.g001

Discussion

In this study, we demonstrated that CHMP2B-positive granules corresponded to GVDs in a variety of neurodegenerative disorders. The GVD nature of these CHMP2B-positive granules was demonstrated on morphological grounds and because of the strong co-localization upon both HE staining and with other GVD markers including pSmad2/3 [38] and Ub [2,26]. In addition, the number of CHMP2B-positive GVDs was comparable with that of neurons with granules immunopositive for the GVD markers (pSmad2/3 and Ub) among the different diseases. Indeed, while GVDs are often assumed to be a pathological entity associated with AD, they have been described within the hippocampus in a number of neurodegenerative diseases; in a preceding investigation, other GVD markers including CK1 delta [17] and p-SAPK/JNK [41] also confirmed the presence of GVDs in the brains of patients with non-AD neurodegenerative disorders. Compared with p-SAPK/JNK, with which immunohistochemistry revealed pathological accumulations of NFTs in addition to GVDs [41], the advantage of CHMP2B as well as CK1 delta as a GVD marker is that it specifically stains GVDs but no other coexisting structures. Taken together, it is reasonable to argue that along with CK1 delta, CHMP2B is a robust marker of GVD in that it specifically detected GVD in AD as well as in non-AD neurodegenerative disorders.

In AD, several lines of evidence have suggested that GVDs appear within the hippocampal pyramidal neurons when phosphorylated tau begins to aggregate into early-stage NFTs [11,15,18,31]; however, whether one can adapt this relationship to non-AD diseases had not yet been systematically examined [42]. In this study, we showed that the number of neurons with CHMP2B-positive GVDs increased in association with phosphorylated tau accumulation in the hippocampus not only in AD but also in a wide range of non-AD neurodegenerative disorders. In addition, we provided direct evidence that diffuse staining for phosphorylated tau could be detected in neurons with CHMP2B-positive GVDs in most of the non-AD cases including PSP and PDD. The pathological forms of tau from AD and PDD patients demonstrate four bands on western blots (72, 68, 64, and 60 kDa; Type I pattern) [43,44], while pathological tau from PSP [45] demonstrates three bands (72, 68, and 64 kDa; Type III pattern). Unfortunately, we could not show colocalization of CHMP2B-positive GVDs with phosphorylated tau in PiD, which demonstrates two bands (64 and 60 kDa; Type II pattern) on western blots [46,47], probably because of the small number of neurons with CHMP2B-positive GVDs. Therefore, our results suggested that in most hippocampal neurons harboring GVDs, they appear in relation to phosphorylated tau accumulation in non-AD neurodegenerative disorders including the 'tauopathies'. However, further studies are needed to clarify whether GVDs appear in relation to phosphorylated tau in tauopathies, irrespective of the phosphorylated tau isoforms.

The most notable finding of the present study is the presence of GVDs in the phosphorylated tau-containing neurons in various neurodegenerative disorders other than AD. Although this finding raises the possibility that there is a common mechanism for GVD formation and phosphorylated tau accumulation, the cellular fates of GVD-harboring neurons may differ between AD and non-AD disorders. Previous studies have suggested that neurons harboring GVDs with phosphorylated tau accumulation reflected 'toxic' or 'apoptotic' alterations in AD [11,18], based on their relationship with phosphorylated tau, whose degree of accumulation correlates with neuronal loss in the hippocampus [42,48,49], as well as the hippocampal vulnerability, both of which have been extensively characterized and documented in AD [50]. Moreover, an exponential relationship exists between the number of GVDs

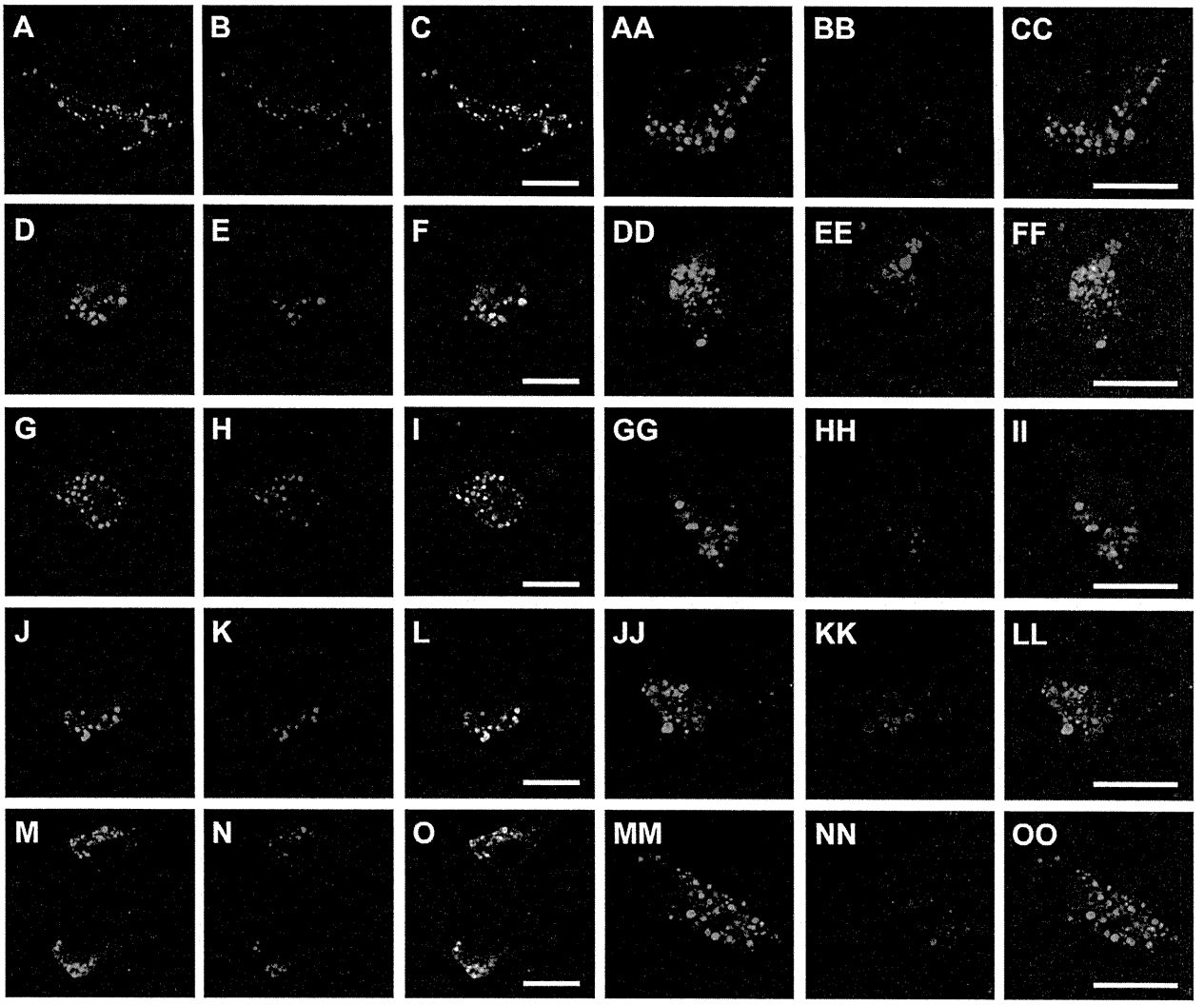

Figure 2. CHMP2B-positive GVDs colocalize with pSmad2/3 and ubiquitin. Hippocampal sections were stained with both anti-CHMP2B antibody (**A, D, G, J, M, AA, DD, GG, JJ, MM**, *green*) and antibodies against pSmad2/3(**B, E, H, K, N**, *red*) or ubiquitin (**BB, EE, HH, KK,** NN, *red*). CHMP2B-positive GVDs colocalized with pSmad2/3 and ubiquitin, although their colocalization rates varied. **C, F, I, L, O, CC, FF, II, LL, OO**, merged images counterstained with Hoechst Dye (*blue*). **A, B, C, AA, BB, CC**, amyotrophic lateral sclerosis; **D, E, F, DD, EE, FF**, pantothenate kinase-associated neurodegeneration; **G, H, I, GG, HH, II**, multiple system atrophy with cerebellar ataxia; **J, K, L, JJ, KK, LL**, progressive supranuclear palsy; **M, N, O, MM, NN, OO**, Parkinson disease with dementia. Scale bars represent 20 μm.
doi:10.1371/journal.pone.0026996.g002

and neuronal loss observed in AD [42]. In contrast, a correlation between tau accumulation and cognitive decline or neuronal loss does not necessarily exist in other disorders [51,52], and it is not known whether the same exponential relationship applies to non-AD cases [42]. Therefore, it is unclear whether hippocampal neurons harboring GVDs with tau accumulation observed in non-AD disorders are pathognomonic for phosphorylated tau-related neurodegeneration, or perhaps are an underlying toxic moiety.

It is unclear whether the presence of phosphorylated tau in the hippocampus of non-AD cases is necessarily more than a result of normal aging. Tau proteins can become insoluble with aging and sometimes contaminate the preparations of the so-called pathological tau aggregates [53]–indeed this contamination has been described in several neurodegenerative diseases [54,55,56]. Moreover, the NFT burden to discriminate between the aging and AD has been thought to be quantitative rather than qualitative [57,58]. Therefore, given that our study lacks age-matched controls, we are uncertain whether the presence of phosphorylated tau in the hippocampus of non-AD cases reflects aging, a substantial AD process, or a disease-specific finding. Nonetheless, strong correlations were observed in our cases between the number of neurons with CHMP2B-positive GVDs and phosphorylated tau burden, even when we excluded AD cases from the analysis. This suggests that, whatever the mechanism involved in phosphorylated tau accumulation, GVDs appear in relation to hippocampal phosphorylated tau accumulation in various neurodegenerative disorders.

Conclusions

In summary, using an antibody to CHMP2B as a molecular label for GVDs [29], we have shown that GVDs appear consistently with hippocampal phosphorylated tau accumulation

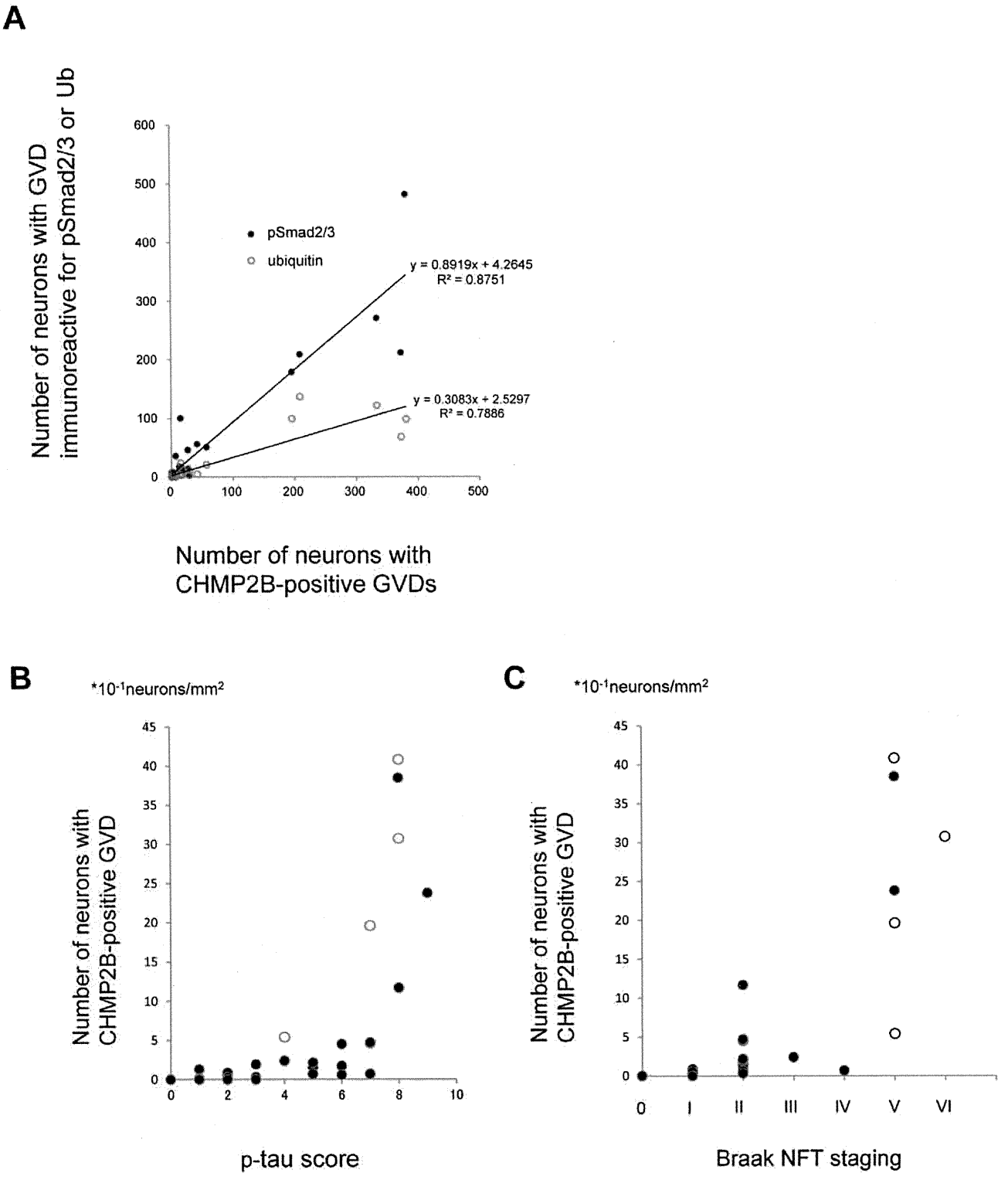

Figure 3. Correlation between the numbers of CHMP2B-positive GVDs with numbers of GVDs immunoreactive for pSmad2/3 or Ub and hippocampal tau pathology. A: Number of neurons with CHMP2B-positive GVDs plotted against those with GVDs immunoreactive for pSmad2/3 (*blue filled circles*) or ubiquitin (Ub; *red open circles*). The Pearson correlation coefficient for pSmad2/3 and ubiquitin was 0.935 ($p<0.01$) and 0.888 ($p<0.01$), respectively, among all the cases studied. Each circle represents an individual hippocampus investigated. **B:** Relationship between phosphorylated tau score (p-tau score) and the number of neurons with CHMP2B-positive GVDs in non-Alzheimer's disease (AD) neurodegenerative disorders. The number of neurons with CHMP2B-positive GVDs increased significantly with the score for phosphorylated tau pathology ($r=0.60$, $p<0.01$). Each *closed circle* represents an individual non-AD hippocampus investigated. Each *open circle* represents an individual hippocampus from an AD case, for reference. **C:** CHMP2B-positive GVD burden in the hippocampus with respect to Braak NFT stage in non-Alzheimer's disease (AD)

neurodegenerative disorders. The number of neurons with CHMP2B-positive GVDs increased significantly with respect to Braak NFT stage ($r = 0.73$, $p<0.01$). Each *closed circle* represents an individual non-AD hippocampus investigated. Each *open circle* represents an individual hippocampus from an AD case for reference.
doi:10.1371/journal.pone.0026996.g003

in various neurodegenerative disorders. Although GVDs in non-AD neurodegenerative disorders have not been studied thoroughly, our results suggested that they are not incidental findings but rather they appear in relation to phosphorylated tau accumulation, further highlighting the role of GVD in the process of phosphorylated tau accumulation.

Materials and Methods

Ethics Statement

The protocols for neuropathological procedures and analysis were approved by and performed under the guidelines of the ethics committee of Hiroshima University Graduate School of Biomedical Sciences. The neurodegenerative disorders and control samples were obtained with the adequate understanding and written informed consent of family members. For this study, all samples were coded and personal information dissociated from the test results. All the data were analyzed anonymously, and all neuropathological procedures and analysis have been conducted according to the principles expressed in the Declaration of Helsinki.

Brain pathology and staining

Four cases of AD, five cases of myotonic dystrophy (MyD), eight cases of amyotrophic lateral sclerosis, two cases of ALS with dementia (ALS-D), three cases of Parkinson disease with dementia (PDD), and one case each of multiple system atrophy with parkinsonism, multiple system atrophy with cerebellar ataxia (MSA-C), PiD, PSP, CBD, and PKAN, and nine control cases without neurodegenerative disorders according to clinical history and confirmed by thorough neuropathological examination were selected (for case demographics see Table S1, postmortem delays 4–24 hours).

Formalin-fixed, paraffin-embedded tissues including the hippocampus and the parahippocampal gyrus were sliced at a thickness of 7 μm. The sections were deparaffinized and then immunostained with primary antibody. The primary antibodies used were as follows: rabbit polyclonal antibody to CHMP2B (ab33174, dilution 1:600; Abcam, Cambridge, UK); mouse monoclonal antibody to ubiquitin (MAB1510, dilution 1:2,000; Chemicon, Temecula, CA); goat polyclonal antibody to pSmad2/3 (sc-11769, dilution 1:400; Santa Cruz Biotech, Santa Cruz, CA); and mouse monoclonal antibody to phosphorylated tau (AT8, dilution 1:800; Innogenetics, Gent, Belgium). For antigen retrieval, the slides were microwaved in distilled water for 10 min then washed in phosphate-buffered saline (PBS) for 5 min. Deparaffinized sections were then incubated with 1% H_2O_2 in methanol for 20 min to eliminate endogenous peroxidase activity. Each section was incubated with primary antibody overnight at 4°C. After washing in PBS, the sections were incubated with horseradish peroxidase (HRP)-conjugated goat anti-mouse antibody or goat anti-rabbit antibody (both diluted 1:100; DAKO, Glostrup, Denmark) for 30 min at room temperature. The sections were then washed three times in PBS and incubated at room temperature with 3,3′-diaminobenzidine (DAKO). All sections were counterstained with hematoxylin.

In addition, we performed double staining on sections including those of the hippocampus and the parahippocampal gyrus of the disease cases. We applied the same primary antibodies as described above. These primary antibodies were detected with the following secondary antibodies (dilution 1:500; Molecular Probes, Eugene, OR): Alexa Fluor 488 donkey anti-rabbit IgG, Alexa Fluor 546 donkey anti-mouse IgG, Alexa Fluor 546 donkey anti-goat IgG, Alexa Fluor 488 goat anti-mouse IgG, and Alexa Fluor 546 goat anti-mouse IgG. 0.5% Sudan black in 70% ethanol was used to quench autofluorescence before mounting the paraffin-embedded sections. The slides were mounted with Vectashield (Vector Laboratories, Burlingame, CA), and observed under a fluorescence microscope (BIOREVO BZ-9000; Keyence, Osaka, Japan) or an LSM510 confocal laser scanning microscope (Carl Zeiss AG, Oberkochen, Germany).

We assessed the staining specificity by replacing the primary antibodies with an appropriate amount of non-immune rabbit serum or PBS containing 3% bovine serum albumin or by pre-incubating the primary antibodies with an excess of peptide immunogen. No reaction products were seen in the sections thus treated (data not shown).

Table 1. Scoring system used to quantify neurons with phosphorylated tau.

Structures per field	phosphorylated tau score (p-tau score)
0	0
1–2	1
3–4	2
5–9	3
10–14	4
15–19	5
20–24	6
25–29	7
30–34	8
35–40	9
> 40	10

doi:10.1371/journal.pone.0026996.t001

Quantitative analysis

For all cases, we counted the number of neurons with CHMP2B-positive GVDs and neurons with granules immunopositive for pSmad2/3 and Ub in the hippocampus at 400× magnification. For the analysis of the correlation to the tau pathology, the number of neurons with CHMP2B-positive GVDs was expressed as neurons/mm^2; we used a mean number of three independent measures using light microscopy at 400× magnification and the images of total hippocampal area in each case were measured by the Image J (NIH) software.

The accumulation of phosphorylated tau in the hippocampus was evaluated using the grading score of Mölsä with some modifications [59]. Briefly, AT8-stained sections including the hippocampus were scanned using light microscopy at 100× magnification. Five randomly selected fields, each measuring 0.92 mm^2, were selected, and the mean number of neurons positive for phosphorylated tau in each field was calculated (Table 1). A lesion score was then assigned, ranging from 0 to 10.

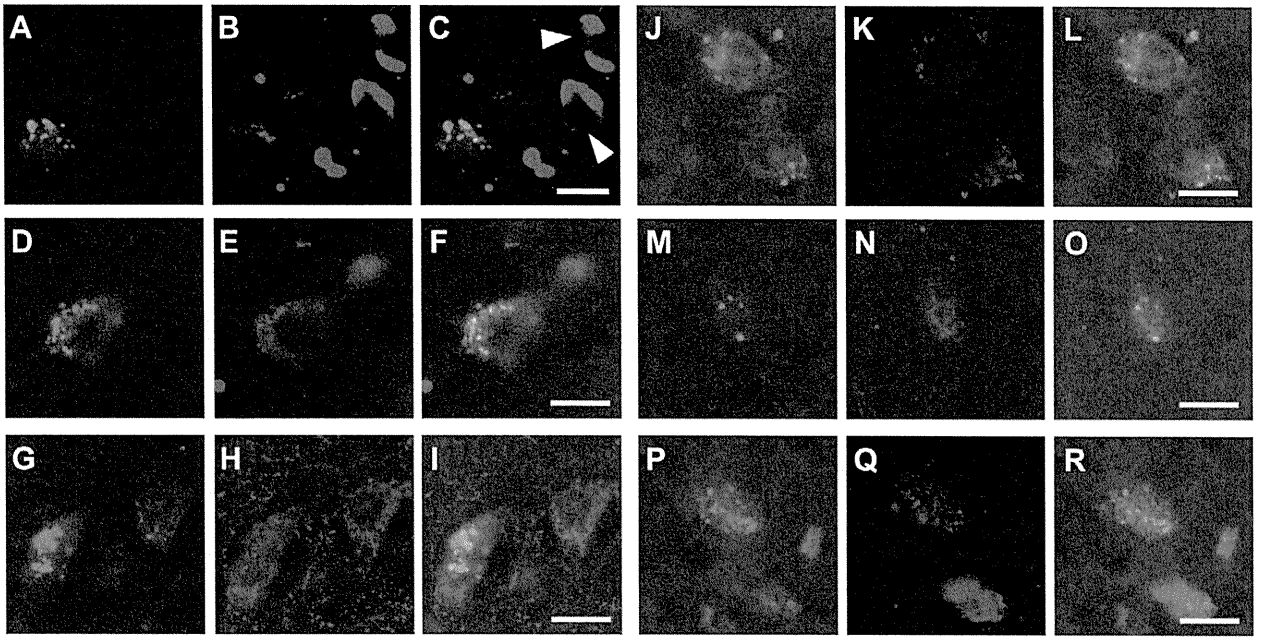

Figure 4. Correlation between CHMP2B-positive GVDs and phosphorylated tau at the cellular level. Double immunofluorescence labeling for CHMP2B (**A, D, G, J, M, P**; *green*), tau phosphorylated at Ser-202 and Thr-205 (**B, E, H, K, N, Q**; *red*), and merged images (**C, F, I, L, O, R**) in sections from patients with several neurodegenerative disorders is shown. Note that, in neurons containing CHMP2B-positive GVDs, diffuse staining for phosphorylated tau could be detected in Alzheimer's disease. In contrast, no co-occurrence of CHMP2B-positive GVDs and phosphorylated tau in tangle-bearing neurons (**arrowheads**) was observed in Alzheimer's disease (**A, B, C**). A similar co-occurrence of CHMP2B-positive GVDs and diffuse staining for phosphorylated tau in neurons was observed in several other neurodegenerative disorders (**D–R**). **D, E, F,** myotonic dystrophy; **G, H, I,** multiple system atrophy with parkinsonism; **J, K, L,** progressive supranuclear palsy; **M, N, O,** Parkinson disease with dementia; **P, Q, R,** pantothenate kinase-associated neurodegeneration. Merged images were counterstained with Hoechst Dye (**F, I, L, O, R**; *blue*). Scale bars represent 20 μm.
doi:10.1371/journal.pone.0026996.g004

For example, if the lowest neurons with phosphorylated tau density were 10–14 and the highest 26–30, the range would be 10–30, giving a midpoint of 20 and phosphorylated tau score (p-tau score) of 6. If the highest density were over 40, the arbitrary figure of 45 was used when calculating the midpoint. Braak staging was determined by AT8 immunostaining of neurofibrillary tangles in hippocampus and isocortical brain regions [60].

Statistical evaluations were performed with the SPSS 14 software package (SPSS, Chicago, Illinois). Due to the exploratory nature of our investigation, the level of significance was set to .05 (two-tailed tests). To avoid effects of aging, we used partial correlations to analyze the relations between number of neurons with CHMP2B-positive GVDs and phosphorylated tau accumulation. Partial correlation analysis reduces the potential for misleading interpretation of data and in the current study, provided a more rigorous investigation of the relationships between the variables. We interpreted coefficients >.5 as strong correlations [61].

Supporting Information

Table S1 Description of cases studied.
(DOC)

Acknowledgments

The authors would like to thank Professor N. Sakai, Department of Molecular and Pharmacological Neuroscience, Hiroshima University Graduate School of Biomedical Sciences, for the use of his facilities and his support. The authors would also like to thank Ms. Y. Furuno, Ms. M. Sasanishi, and Ms. A. Hironaka for their excellent technical assistance; and the Analysis Center of Life Science, Hiroshima University, for the use of its facilities.

Author Contributions

Conceived and designed the experiments: YY TM TK ED MH YN TY MM. Performed the experiments: YY TM. Analyzed the data: YY TM TT. Contributed reagents/materials/analysis tools: TT TY MM. Wrote the paper: YY TM TT.

References

1. Woodard JS (1962) Clinicopathologic significance of granulovacuolar degeneration in Alzheimer's disease. J Neuropathol Exp Neurol 21: 85–91.
2. Okamoto K, Hirai S, Iizuka T, Yanagisawa T, Watanabe M (1991) Reexamination of granulovacuolar degeneration. Acta Neuropathol 82: 340–345.
3. Bondareff W, Wischik CM, Novak M, Roth M (1991) Sequestration of tau by granulovacuolar degeneration in Alzheimer's disease. Am J Pathol 139: 641–647.
4. Dickson DW, Ksiezak-Reding H, Davies P, Yen SH (1987) A monoclonal antibody that recognizes a phosphorylated epitope in Alzheimer neurofibrillary tangles, neurofilaments and tau proteins immunostains granulovacuolar degeneration. Acta Neuropathol 73: 254–258.
5. Ikegami K, Kimura T, Katsuragi S, Ono T, Yamamoto H, et al. (1996) Immunohistochemical examination of phosphorylated tau in granulovacuolar degeneration granules. Psychiatry Clin Neurosci 50: 137–140.
6. Mena R, Robitaille Y, Cuello AC (1992) New patterns of intraneuronal accumulation of the microtubular binding domain of tau in granulovacuolar degeneration. J Geriatr Psychiatry Neurol 5: 132–141.
7. Gamblin TC, Chen F, Zambrano A, Abraha A, Lagalwar S, et al. (2003) Caspase cleavage of tau: linking amyloid and neurofibrillary tangles in Alzheimer's disease. Proc Natl Acad Sci U S A 100: 10032–10037.
8. Gervais FG, Xu D, Robertson GS, Vaillancourt JP, Zhu Y, et al. (1999) Involvement of caspases in proteolytic cleavage of Alzheimer's amyloid-beta

precursor protein and amyloidogenic A beta peptide formation. Cell 97: 395–406.
9. Jellinger KA, Stadelmann C (2000) Mechanisms of cell death in neurodegenerative disorders. J Neural Transm Suppl 59: 95–114.
10. Selznick LA, Holtzman DM, Han BH, Gokden M, Srinivasan AN, et al. (1999) In situ immunodetection of neuronal caspase-3 activation in Alzheimer disease. J Neuropathol Exp Neurol 58: 1020–1026.
11. Stadelmann C, Deckwerth TL, Srinivasan A, Bancher C, Bruck W, et al. (1999) Activation of caspase-3 in single neurons and autophagic granules of granulovacuolar degeneration in Alzheimer's disease. Evidence for apoptotic cell death. Am J Pathol 155: 1459–1466.
12. Su JH, Kesslak JP, Head E, Cotman CW (2002) Caspase-cleaved amyloid precursor protein and activated caspase-3 are co-localized in the granules of granulovacuolar degeneration in Alzheimer's disease and Down's syndrome brain. Acta Neuropathol 104: 1–6.
13. Ghoshal N, Smiley JF, DeMaggio AJ, Hoekstra MF, Cochran EJ, et al. (1999) A new molecular link between the fibrillar and granulovacuolar lesions of Alzheimer's disease. Am J Pathol 155: 1163–1172.
14. Ishizawa T, Sahara N, Ishiguro K, Kersh J, McGowan E, et al. (2003) Co-localization of glycogen synthase kinase-3 with neurofibrillary tangles and granulovacuolar degeneration in transgenic mice. Am J Pathol 163: 1057–1067.
15. Kannanayakal TJ, Tao H, Vandre DD, Kuret J (2006) Casein kinase-1 isoforms differentially associate with neurofibrillary and granulovacuolar degeneration lesions. Acta Neuropathol 111: 413–421.
16. Leroy K, Boutajangout A, Authelet M, Woodgett JR, Anderton BH, et al. (2002) The active form of glycogen synthase kinase-3beta is associated with granulovacuolar degeneration in neurons in Alzheimer's disease. Acta Neuropathol 103: 91–99.
17. Schwab C, DeMaggio AJ, Ghoshal N, Binder LI, Kuret J, et al. (2000) Casein kinase 1 delta is associated with pathological accumulation of tau in several neurodegenerative diseases. Neurobiol Aging 21: 503–510.
18. Hoozemans JJ, van Haastert ES, Nijholt DA, Rozemuller AJ, Eikelenboom P, et al. (2009) The unfolded protein response is activated in pretangle neurons in Alzheimer's disease hippocampus. Am J Pathol 174: 1241–1251.
19. Kadokura A, Yamazaki T, Kakuda S, Makioka K, Lemere CA, et al. (2009) Phosphorylation-dependent TDP-43 antibody detects intraneuronal dot-like structures showing morphological characters of granulovacuolar degeneration. Neurosci Lett 463: 87–92.
20. Amador-Ortiz C, Lin WL, Ahmed Z, Personett D, Davies P, et al. (2007) TDP-43 immunoreactivity in hippocampal sclerosis and Alzheimer's disease. Ann Neurol 61: 435–445.
21. Higashi S, Iseki E, Yamamoto R, Minegishi M, Hino H, et al. (2007) Concurrence of TDP-43, tau and alpha-synuclein pathology in brains of Alzheimer's disease and dementia with Lewy bodies. Brain Res 1184: 284–294.
22. Hu WT, Josephs KA, Knopman DS, Boeve BF, Dickson DW, et al. (2008) Temporal lobar predominance of TDP-43 neuronal cytoplasmic inclusions in Alzheimer disease. Acta Neuropathol 116: 215–220.
23. Josephs KA, Whitwell JL, Knopman DS, Hu WT, Stroh DA, et al. (2008) Abnormal TDP-43 immunoreactivity in AD modifies clinicopathologic and radiologic phenotype. Neurology 70: 1850–1857.
24. Kadokura A, Yamazaki T, Lemere CA, Takatama M, Okamoto K (2009) Regional distribution of TDP-43 inclusions in Alzheimer disease (AD) brains: their relation to AD common pathology. Neuropathology 29: 566–573.
25. Uryu K, Nakashima-Yasuda H, Forman MS, Kwong LK, Clark CM, et al. (2008) Concomitant TAR-DNA-binding protein 43 pathology is present in Alzheimer disease and corticobasal degeneration but not in other tauopathies. J Neuropathol Exp Neurol 67: 555–564.
26. Love S, Saitoh T, Quijada S, Cole GM, Terry RD (1988) Alz-50, ubiquitin and tau immunoreactivity of neurofibrillary tangles, Pick bodies and Lewy bodies. J Neuropathol Exp Neurol 47: 393–405.
27. Ghanevati M, Miller CA (2005) Phospho-beta-catenin accumulation in Alzheimer's disease and in aggresomes attributable to proteasome dysfunction. J Mol Neurosci 25: 79–94.
28. Holzer M, Gartner U, Stobe A, Hartig W, Gruschka H, et al. (2002) Inverse association of Pin1 and tau accumulation in Alzheimer's disease hippocampus. Acta Neuropathol 104: 471–481.
29. Yamazaki Y, Takahashi T, Hiji M, Kurashige T, Izumi Y, et al. (2010) Immunopositivity for ESCRT-III subunit CHMP2B in granulovacuolar degeneration of neurons in the Alzheimer's disease hippocampus. Neurosci Lett 477: 86–90.
30. Funk KE, Mrak RE, Kuret J (2010) Granulovacuolar Degeneration Bodies of Alzheimer's Disease Resemble Late-stage Autophagic Organelles. Neuropathol Appl Neurobiol.
31. Lagalwar S, Guillozet-Bongaarts AL, Berry RW, Binder LI (2006) Formation of phospho-SAPK/JNK granules in the hippocampus is an early event in Alzheimer disease. J Neuropathol Exp Neurol 65: 455–464.
32. Ball MJ (1978) Topographic distribution of neurofibrillary tangles and granulovacuolar degeneration in hippocampal cortex of aging and demented patients. A quantitative study. Acta Neuropathol 42: 73–80.
33. Steele JC, Richardson JC, Olszewski J (1964) Progressive Supranuclear Palsy. A Heterogeneous Degeneration Involving the Brain Stem, Basal Ganglia and Cerebellum with Vertical Gaze and Pseudobulbar Palsy, Nuchal Dystonia and Dementia. Arch Neurol 10: 333–359.
34. Eidelberg D, Sotrel A, Joachim C, Selkoe D, Forman A, et al. (1987) Adult onset Hallervorden-Spatz disease with neurofibrillary pathology. A discrete clinicopathological entity. Brain 110 (Pt 4): pp 993–1013.
35. Gibb WR, Luthert PJ, Marsden CD (1989) Corticobasal degeneration. Brain 112 (Pt 5): pp 1171–1192.
36. Towfighi J (1972) Early Pick's disease. A light and ultrastructural study. Acta Neuropathol 21: 224–231.
37. Filimonenko M, Stuffers S, Raiborg C, Yamamoto A, Malerod L, et al. (2007) Functional multivesicular bodies are required for autophagic clearance of protein aggregates associated with neurodegenerative disease. J Cell Biol 179: 485–500.
38. Chalmers KA, Love S (2007) Neurofibrillary tangles may interfere with Smad 2/3 signaling in neurons. J Neuropathol Exp Neurol 66: 158–167.
39. Xu M, Shibayama H, Kobayashi H, Yamada K, Ishihara R, et al. (1992) Granulovacuolar degeneration in the hippocampal cortex of aging and demented patients–a quantitative study. Acta Neuropathol 85: 1–9.
40. Spillantini MG, Tolnay M, Love S, Goedert M (1999) Microtubule-associated protein tau, heparan sulphate and alpha-synuclein in several neurodegenerative diseases with dementia. Acta Neuropathol 97: 585–594.
41. Lagalwar S, Berry RW, Binder LI (2007) Relation of hippocampal phospho-SAPK/JNK granules in Alzheimer's disease and tauopathies to granulovacuolar degeneration bodies. Acta Neuropathol 113: 63–73.
42. Ball MJ (1977) Neuronal loss, neurofibrillary tangles and granulovacuolar degeneration in the hippocampus with ageing and dementia. A quantitative study. Acta Neuropathol 37: 111–118.
43. Flament S, Delacourte A, Mann DM (1990) Phosphorylation of Tau proteins: a major event during the process of neurofibrillary degeneration. A comparative study between Alzheimer's disease and Down's syndrome. Brain Res 516: 15–19.
44. Vermersch P, Delacourte A, Javoy-Agid F, Hauw JJ, Agid Y (1993) Dementia in Parkinson's disease: biochemical evidence for cortical involvement using the immunodetection of abnormal Tau proteins. Ann Neurol 33: 445–450.
45. Schmidt ML, Huang R, Martin JA, Henley J, Mawal-Dewan M, et al. (1996) Neurofibrillary tangles in progressive supranuclear palsy contain the same tau epitopes identified in Alzheimer's disease PHFtau. J Neuropathol Exp Neurol 55: 534–539.
46. Buee Scherrer V, Hof PR, Buee L, Leveugle B, Vermersch P, et al. (1996) Hyperphosphorylated tau proteins differentiate corticobasal degeneration and Pick's disease. Acta Neuropathol 91: 351–359.
47. Lieberman AP, Trojanowski JQ, Lee VM, Balin BJ, Ding XS, et al. (1998) Cognitive, neuroimaging, and pathological studies in a patient with Pick's disease. Ann Neurol 43: 259–265.
48. Arriagada PV, Growdon JH, Hedley-Whyte ET, Hyman BT (1992) Neurofibrillary tangles but not senile plaques parallel duration and severity of Alzheimer's disease. Neurology 42: 631–639.
49. Bondareff W, Mountjoy CQ, Roth M, Hauser DL (1989) Neurofibrillary degeneration and neuronal loss in Alzheimer's disease. Neurobiol Aging 10: 709–715.
50. Braak H, Braak E (1991) Neuropathological stageing of Alzheimer-related changes. Acta Neuropathol 82: 239–259.
51. Kiuchi A, Otsuka N, Namba Y, Nakano I, Tomonaga M (1991) Presenile appearance of abundant Alzheimer's neurofibrillary tangles without senile plaques in the brain in myotonic dystrophy. Acta Neuropathol 82: 1–5.
52. Gertz HJ, Xuereb JH, Huppert FA, Brayne C, Kruger H, et al. (1996) The relationship between clinical dementia and neuropathological staging (Braak) in a very elderly community sample. European Archives of Psychiatry and Clinical Neuroscience 246: 132–136.
53. Bronner IF, ter Meulen BC, Azmani A, Severijnen LA, Willemsen R, et al. (2005) Hereditary Pick's disease with the G272V tau mutation shows predominant three-repeat tau pathology. Brain 128: 2645–2653.
54. Hof PR, Bouras C, Buee L, Delacourte A, Perl DP, et al. (1992) Differential distribution of neurofibrillary tangles in the cerebral cortex of dementia pugilistica and Alzheimer's disease cases. Acta Neuropathol 85: 23–30.
55. Hof PR, Charpiot A, Delacourte A, Buee L, Purohit D, et al. (1992) Distribution of neurofibrillary tangles and senile plaques in the cerebral cortex in postencephalitic parkinsonism. Neurosci Lett 139: 10–14.
56. Hof PR, Delacourte A, Bouras C (1992) Distribution of cortical neurofibrillary tangles in progressive supranuclear palsy: a quantitative analysis of six cases. Acta Neuropathol 84: 45–51.
57. Arriagada PV, Marzloff K, Hyman BT (1992) Distribution of Alzheimer-type pathologic changes in nondemented elderly individuals matches the pattern in Alzheimer's disease. Neurology 42: 1681–1688.
58. Tomlinson BE, Blessed G, Roth M (1970) Observations on the brains of demented old people. J Neurol Sci 11: 205–242.
59. Molsa PK, Sako E, Paljarvi L, Rinne JO, Rinne UK (1987) Alzheimer's disease: neuropathological correlates of cognitive and motor disorders. Acta Neurol Scand 75: 376–384.
60. Braak H, Alafuzoff I, Arzberger T, Kretzschmar H, Del Tredici K (2006) Staging of Alzheimer disease-associated neurofibrillary pathology using paraffin sections and immunocytochemistry. Acta Neuropathol 112: 389–404.
61. Cohen J (1988) Statistical power analysis for the behavioral sciences. Hillsdale, ed. N.J: L. Erlbaum Associates. xxi, 567 p.

INTERNAL MEDICINE

□ CASE REPORT □

Two Cases of Cerebral Embolism Caused by Apical Thrombi in Midventricular Obstructive Cardiomyopathy

Ikuko Takeda[1], Mayu Sekine[2], Hayato Matsushima[3], Naohisa Hosomi[1], Takeshi Nakamura[1], Toshiho Ohtsuki[1], Takemori Yamawaki[1] and Masayasu Matsumoto[1]

Abstract

Midventricular obstructive hypertrophic cardiomyopathy (MOHC) is a rare form of cardiomyopathy that was demonstrated to have caused embolic stroke in two patients. In both cases, the embolic sources of stroke were thrombi in an apical aneurysm caused by turbulent stasis of blood flow and subsequent injury of myocardial endocardium. Even without atrial fibrillation, apical aneurysm can induce emboligenic stroke in MOHC.

Key words: cerebrovascular disease/stroke, midventricular obstructive cardiomyopathy, apical thrombus

(Intern Med 50: 1059-1060, 2011)
(DOI: 10.2169/internalmedicine.50.5079)

Introduction

Most patients with hypertrophic cardiomyopathy (HCM) have asymmetric septal hypertrophy and subaortic obstruction. Midventricular obstructive hypertrophic cardiomyopathy (MOHC) presents as atypical intraluminal stenosis of the midventricle followed by a pressure gradient between the apical and basal chambers. A previous study reported the incidence of concealed apical aneurysm with midventricular cavity obliteration to be approximately 1.5% of all HCM cases (1). Atrial fibrillation and the dilated phase of HCM are associated with embolic stroke (2); however, in 9.8% of cases of HCM, a definite origin of stroke could not be identified (3). We describe herein two MOHC patients with cerebral embolism induced by apical thrombi.

Case Report

Case 1

A 42-year-old woman who had MOHC was hospitalized because of nausea and difficulty speaking. On arrival, she had right facial palsy, dysarthria and ataxia of the right extremities. Laboratory data revealed an increased white blood cell count (12,400/mm^3), D-dimer (1.1 μg/mL), and N-terminal proBNP (3484 pg/mL). Electrocardiography (ECG) on admission showed a sinus rhythm with deep T wave inversion. MRI showed acute cerebellar infarcts and occlusion of the basilar artery (Fig. 1). Transthoracic echocardiography revealed a left midventricular obstruction followed by the apical aneurysm; on ultrasound contrast, a mural thrombal defect was observed (Fig. 1). Transesophageal echocardiography did not demonstrate the apical thrombus or any other sources of embolus. Eight days after admission, MRI revealed left cerebellar, right pontine, and left cerebral peduncle infarcts. The patient was treated with unfractionated heparin and warfarin, and her symptoms gradually improved.

Case 2

A 65-year-old man was admitted with syncope and was diagnosed with ventricular tachycardia and midventricular obstructive cardiomyopathy. On the third day after admission, he had left hemiparesis, dysarthria and unilateral spatial neglect. Laboratory data revealed increases in blood sugar (376 mg/dL), D-dimer (4.0 μg/mL), and BNP (717 pg/mL). ECG detected a sinus rhythm with a deep negative T inversion in leads V3-V6. CT showed no infarction and perfusion CT demonstrated hypoperfusion and a prolonged

[1]Department of Clinical Neuroscience and Therapeutics, Hiroshima University, Graduate School of Biomedical Sciences, Japan, [2]Department of Neurology, Tokyo Saiseikai Central Hospital, Japan and [3]Cerebrovascular Division, National Cerebral and Cardiovascular Center, Japan
Received for publication December 27, 2010; Accepted for publication January 24, 2011
Correspondence to Dr. Ikuko Takeda, itakeda@hiroshima-u.ac.jp

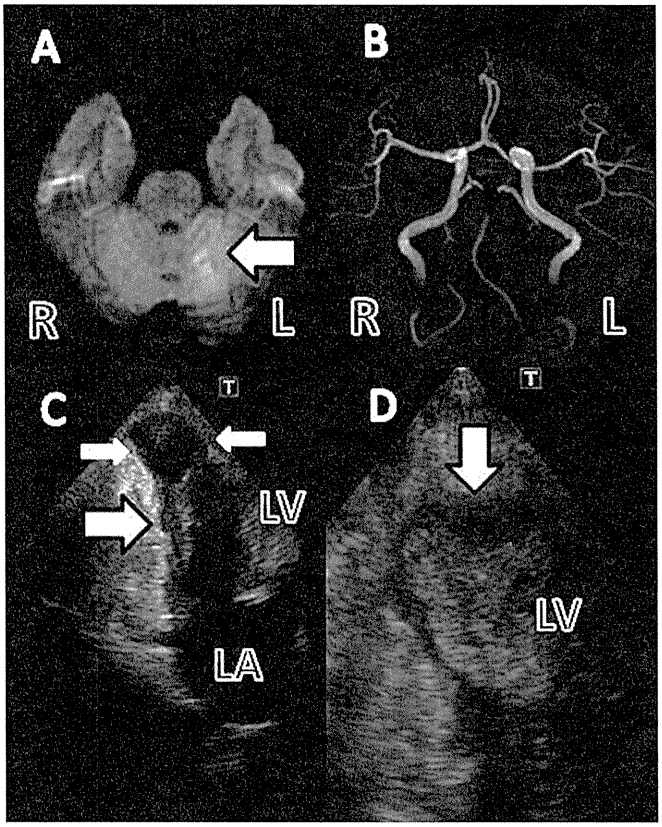

Figure 1. **MRI and transthoracic echocardiography in Case 1. (A) Diffusion-weighted imaging showed high intensity signals in cerebellum (arrow) on arrival. (B) MRA showing the top of the basilar artery occluded on arrival. (C) Transthoracic echocardiography demonstrated midventricular obstruction in systole (large arrow) and the apical aneurysm (small arrow). (D) Transthoracic echocardiography with contrast showed a thrombal defect (arrow) in the apical aneurysm.**

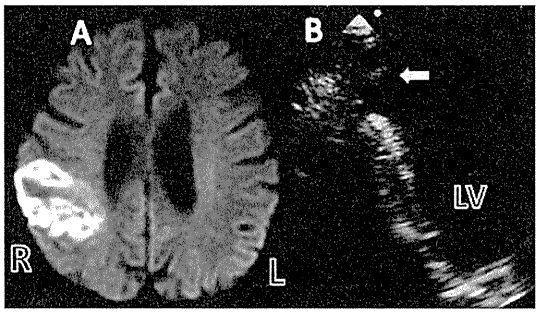

Figure 2. **MRI and transthoracic echocardiography in Case 2. (A) Diffusion-weighted imaging showed a high intensity signal in the right frontotemporal lobe. (B) Transthoracic echocardiography revealed a thrombus (arrow) in the apical aneurysm.**

mean transit time (MTT) in the right frontotemporal lobe. Transthoracic echocardiography revealed two thrombi on an apical aneurysm (Fig. 2) and continuous wave Doppler recorded the paradoxical diastolic flow from the apex to the base of the left ventricular cavity. One hour and 37 minutes later, the patient was treated with intravenous thrombolysis with tissue plasminogen activator and his condition improved. Warfarin was administered to prevent recurrence.

Discussion

Among the cases of HCM, the main cause of ischemic stroke is atrial fibrillation and the dilated phase of HCM (3). Paroxysmal or chronic atrial fibrillation ultimately occurs in 20% to 25% of HCM patients (4, 5) and causes 23% of the cumulative incidence of vascular events (2). We encountered and thoroughly examined two cases of stroke, possibly caused by a thrombus of akinetic apical aneurysm as possible sources of embolism. Few patients with normal left ventricular systolic performance who have never experienced stroke have demonstrated thrombus in an apical aneurysm (6). A thrombus is induced by turbulent stasis of blood flow and injured myocardial endocardium by both systolic midventricular obstruction and diastolic paradoxical jet flow (7, 8) from the apex to the base of the left ventricular cavity.

Transthoracic echocardiography was superior to transesophageal echocardiography in revealing the thrombus of apical aneurysm in Case 1. Because apical thrombi can cause emboli, MOHC patients without atrial fibrillation require transthoracic echocardiography to locate embolic sources.

The authors state that they have no Conflict of Interest (COI).

References

1. Maron MS, Finley JJ, Bos JM, et al. Prevalence, clinical significance, and natural history of left ventricular apical aneurysms in hypertrophic cardiomyopathy. Circulation **118**: 1541-1549, 2008.
2. Maron BJ, Olivotto L, Bellone P, et al. Clinical profile of stroke in 900 patients with hypertrophic cardiomyopathy. JACC **39**: 301-307, 2002.
3. Maron BJ. Hypertrophic cardiomyopathy. JAMA **287**: 1308-1315, 2002.
4. Maron BJ, Casey SA, Poliac LC, Gohman TE, Almquist AK, Aeppli DM. Clinical course of hypertrophic cardiomyopathy in a regional United States cohort. JAMA **281**: 650-655, 1999.
5. Olivotto I, Cecchi F, Casey SA, Dolara A, Traverse JH, Maron BJ. Impact of atrial fibrillation on the clinical course of hypertrophic cardiomyopathy. Circuration **104**: 2517-2524, 2001.
6. Sato Y, Matsumoto N, Matsuo S, et al. Mid-ventricular obstructive hypertrophic cardiomyopathy associated with an apical aneurysm: evaluation of possible causes of aneurysm formation. Yonsei Med J **48**: 879-882, 2007.
7. Cooke JC, Cotton JM, Monaghan MJ. Mid-ventricular HOCM with apical asynergy. Heart **83**: 51, 2000.
8. Mixon TA, Giebel DW. Abnormal diastolic flow demonstrated by color M mode echocardiography in hypertrophic cardiomyopathy with mid-ventricular cavity obliteration. Echocardiography **21**: 49-53, 2004.

© 2011 The Japanese Society of Internal Medicine
http://www.naika.or.jp/imindex.html

ELSEVIER

Brain & Development xxx (2011) xxx–xxx

BRAIN & DEVELOPMENT
Official Journal of the Japanese Society of Child Neurology

www.elsevier.com/locate/braindev

Case report

Posterior cerebral artery dissection on a serial magnetic resonance angiography

Toshiki Takenouchi [a,*], Sachiko Shimozato [a], Hirokazu Fujiwara [b], Suketaka Momoshima [b], Takao Takahashi [a]

[a] *Department of Pediatrics, Keio University Hospital, Keio University School of Medicine, Tokyo, Japan*
[b] *Department of Radiology, Keio University Hospital, Keio University School of Medicine, Tokyo, Japan*

Received 20 May 2011; received in revised form 21 June 2011; accepted 22 June 2011

Abstract

Posterior cerebral artery (PCA) dissection in children seldom is reported in the literature. This is the second report of acute PCA dissection with infarct occurring in a young child. A serial magnetic resonance angiography demonstrated a delayed and transient narrowing of the arterial caliber, which was consistent with a focal PCA dissection with delayed vascular recanalization. PCA dissection should be included in the causes of infarct in children and a thorough and serial neurovascular imaging should be considered if no cause of stroke is found.
© 2011 The Japanese Society of Child Neurology. Published by Elsevier B.V. All rights reserved.

Keywords: Posterior cerebral artery; Arterial dissection; Infarct

1. Background

Posterior cerebral artery (PCA) dissection is extremely rare but an importance case of stroke [1–5]. Here we report a pediatric case of right thalamic infarct secondary to right PCA dissection noted on a serial magnetic resonance angiography (MRA) to discuss its underlying pathophysiology and future clinical implications.

2. Case presentation

The case was a three-year-old ambidextrous girl, whose past medical and family history was non-contributory.

She was in her usual-state-of-health and playing with her brother at home. When her mother at kitchen heard a sudden screaming, her mother quickly ran to find her lying down on the floor in front of a door. There was no loss of consciousness. She was holding back of her head and right neck and complained of severe pain. Since her mother thought that she hit her head against the doorknob, she was lain down on a bed. However she did not have any improvement in her headache over the next several hours. She was taken to a local emergency room, where she was noted to have a left hemiparesis involving her left face, arm and leg (day 0). There was no bruise on physical examination, fracture on skull X-rays or intracranial hemorrhage on head CT scan.

Abbreviations: MRA, magnetic resonance angiography; MRI, magnetic resonance imaging; PCA, posterior cerebral artery; PLIC, posterior limb of internal capsule; T, tesla

* Corresponding author. Address: Department of Pediatrics, Keio University Hospital, Keio University School of Medicine, 35 Shinanomachi, Shinjuku-ku, Tokyo 1608582, Japan. Tel.: +81 03 3353 1211; fax: +81 03 5379 1978.
E-mail address: toshiki.take@z5.keio.jp (T. Takenouchi).

0387-7604/$ - see front matter © 2011 The Japanese Society of Child Neurology. Published by Elsevier B.V. All rights reserved.
doi:10.1016/j.braindev.2011.06.012

Please cite this article in press as: Takenouchi T et al. Posteriorcerebral artery dissection on aserial magnetic resonance angiography. Brain Dev (2011), doi:10.1016/j.braindev.2011.06.012

A magnetic resonance imaging (MRI) of the brain approximately 22 h after the symptom onset (day 1) demonstrated restricted diffusion in the right thalamus and posterior limb of internal capsule (PLIC), consistent with acute arterial infarct (Fig. 1A). An MRA of the brain utilizing a magnetic field strength of 1.5 Tesla (T) showed minimal narrowing of the right proximal PCA i.e. P1-2 segment, just proximal to the origin of the thalamogeniculate arteries leading to the infarction (Fig. 2A). An MRA of the neck was unremarkable. A follow-up 3T-MRA on day 9 demonstrated a segmental severe stenosis in the same region (Fig. 2B). Another follow-up 3T-MRA on day 37 demonstrated partial resolution of the right P1-2 stenosis (Fig. 2C) indicating vascular recanalization. An MRI showed cystic changes with gliosis in the right lateral thalamus sparing the

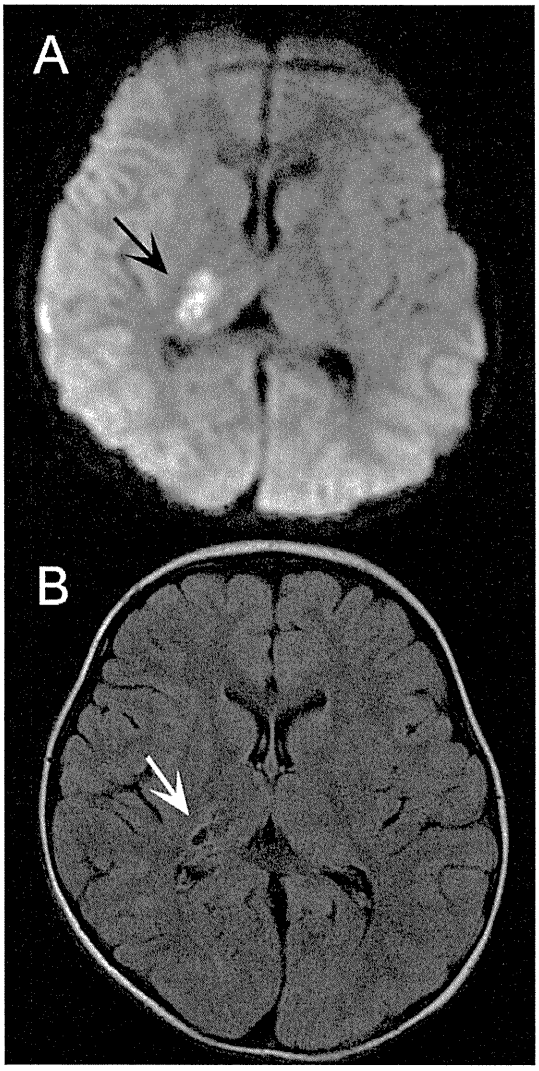

Fig. 1. Brain magnetic resonance imagings. (A) An axial diffusion-weighted image on day 1 demonstrating restricted diffusion in the right lateral thalamus and posterior limb of internal capsule consistent with acute arterial infarct (black arrow). (B) An axial fluid-attenuated-inversion-recovery image on day 37 showing cystic changes with gliosis in the right lateral thalamus (white arrow), confirming posterior circulation infarct.

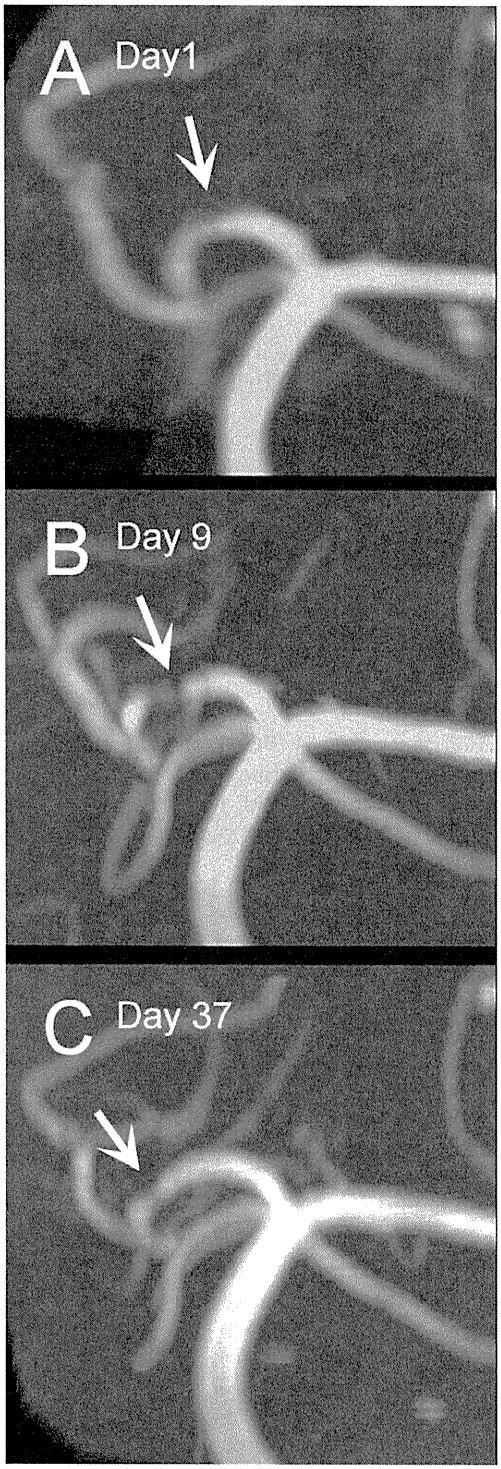

Fig. 2. A serial magnetic resonance angiography (MRA) from day 1 through 37. (A) A 1.5T-MRA on day 1. Note a minimal caliber change in the P1-2 segment of the right posterior cerebral artery (arrow). (B) A 3T-MRA on day 9. Note a segmental discontinuity suggestive of severe stenosis in the same region (arrow). (C) A 3T-MRA on day 37. Note partial resolution of the caliber change with tapered appearance indicating partial recanalization of the arterial dissection (arrow).

Please cite this article in press as: Takenouchi T et al. Posteriorcerebral artery dissection on aserial magnetic resonance angiography. Brain Dev (2011), doi:10.1016/j.braindev.2011.06.012

PLIC, which confirmed that the infarct occurred within the territory of right PCA (Fig. 1B).

An extensive cardiovascular and hematological testings did not reveal any source of thrombi or emboli or any coagulation abnormalities. Conventional angiography was deliberately not performed after the discussion with her family, given its potential procedural and radiation risks.

The patient was treated with oral aspirin to show a significant and monophasic recovery in her motor strength during and after the hospital course. Her weakness almost completely resolved by 6 months after the symptom onset with no recurrence of the symptoms.

3. Discussion

This is the second report of PCA dissection in young pediatric population. There have been several cases of PCA dissection in adults and anterior circulation stroke in the basal ganglia and thalamus after minor head trauma in children [1–5]. However, there is only one prior report of two young children with PCA dissection in the literature. Thus, Sherman et al. described a seven-year-old girl with PCA dissection occurred after minor head trauma and a 19-month-old boy with PCA dissection without a clear preceding history of trauma [2].

The present case had several reasons suggestive of arterial dissection rather than vasospasm or other etiologies. First, the present case had a segmental PCA stenosis which progressed towards the second week and then gradually improved over at least one month. In a study of 27 head injured children, middle cerebral artery velocity by daily Transcranial Doppler measurements started increasing between the 2nd and 4th day after injury and lasted on average for 4 days. The longest period of increased velocity values lasted 7 days and the shortest, 1 day [6]. While vasospasm tends to have a radiographic appearance with smooth caliber changes, arterial dissection can have characteristic geometry changes such as irregular stenosis, segmental stenosis, and aneurysm formation. The radiographic findings can change dramatically over the period of days or even hours, about 90% of stenoses eventually resolve and two-thirds of occlusions are recanalized [7]. The much longer duration of P1-2 stenosis and its geometric changes in the present case strongly favor arterial dissection with delayed recanalization of the false lumen as the most plausible explanation.

Secondly, arterial infarct due to delayed vasospasm can occur after severe head trauma, which is usually severe enough to cause intracranial hemorrhage [8]. But the present case had no loss of consciousness, skull fracture or intracranial hemorrhage.

Thirdly, patients with arterial dissection present with infarct rather than transient ischemic attacks [9]. In children, pain is not as a prominent feature for arterial dissection as in adults, but still reported in half of the patients [10]. The present case complained of headache and had a complete infarct, which are consistent with intracranial arterial dissections.

As seen in the present case, PCA dissections most commonly occur near the P1-2 junction. It could be particularly vulnerable to shearing and stretching forces, because vertebrobasilar-PCA acutely change its direction posteriorly at P1-2 segment and it is anatomically close to the free border of the tentorium cerebelli [2,5]. Although the present case did not have a witnessed trauma, it was highly likely that she had some preceding traumatic event to her head and/or neck given the circumstances.

It could be argued that conventional angiography remains the gold standard technique in diagnosing vascular anomaly. Although it is true MRA, either in source or reconstructed images, can have limitations in assessing small caliber vessels and conventional angiography provides better angiographic resolution [2], conventional angiography carries substantial procedural and radiation risks especially in children. Thus, we utilized a serial 3T-MRA under sedation to follow caliber changes without significant motion artifact or major complication.

The causes of stroke in children are more divergent and less often identified than those in adults. Since the present case had a barely noticeable P1-2 caliber change on the first 1.5T-MRA, her PCA dissection could have been overlooked without subsequent 3T-MRA studies.

In conclusion, the present case not only demonstrates that PCA dissection can occur in children, but also reinforces that a thorough and repeat neurovascular imaging should be considered if no cause of stroke is detected.

References

[1] Berthier E, Bourrat C. Dissecting aneurysm of the posterior cerebral artery: case report and review of the literature. Cerebrovasc Dis 1993;3:56–9.

[2] Sherman P, Oka M, Aldrich E, Jordan L, Gailloud P. Isolated posterior cerebral artery dissection: report of three cases. AJNR Am J Neuroradiol 2006;27:648–52.

[3] Fisher CM, Ojemann RG, Roberson GH. Spontaneous dissection of cervico-cerebral arteries. Can J Neurol Sci 1978;5:9–19.

[4] Maillo A, Diaz P, Morales F. Dissecting aneurysm of the posterior cerebral artery: spontaneous resolution. Neurosurgery 1991;29:291–4.

[5] Lazinski D, Willinsky RA, TerBrugge K, Montanera W. Dissecting aneurysms of the posterior cerebral artery: angioarchitecture and a review of the literature. Neuroradiology 2000;42:128–33.

[6] Mandera M, Larysz D, Wojtacha M. Changes in cerebral hemodynamics assessed by transcranial Doppler ultrasonography in children after head injury. Childs Nerv Syst 2002;18:124–8.

[7] Schievink WI. Spontaneous dissection of the carotid and vertebral arteries. N Engl J Med 2001;344:898–906.

Please cite this article in press as: Takenouchi T et al. Posteriorcerebral artery dissection on aserial magnetic resonance angiography. Brain Dev (2011), doi:10.1016/j.braindev.2011.06.012

[8] Martin NA, Doberstein C, Zane C, Caron MJ, Thomas K, Becker DP. Posttraumatic cerebral arterial spasm: transcranial Doppler ultrasound, cerebral blood flow, and angiographic findings. J Neurosurg 1992;77:575–83.

[9] Caplan LR. Dissections of brain-supplying arteries. Nat Clin Pract Neurol 2008;4:34–42.

[10] Fullerton HJ, Johnston SC, Smith WS. Arterial dissection and stroke in children. Neurology 2001;57:1155–60.

Please cite this article in press as: Takenouchi T et al. Posteriorcerebral artery dissection on aserial magnetic resonance angiography. Brain Dev (2011), doi:10.1016/j.braindev.2011.06.012

Spine

SPINE Volume 36, Number 4, pp E256–E262
©2011, Lippincott Williams & Wilkins

CERVICAL SPINE

Remodeling of C2 Facet Deformity Prevents Recurrent Subluxation in Patients With Chronic Atlantoaxial Rotatory Fixation

A Novel Strategy for Treatment of Chronic Atlantoaxial Rotatory Fixation

Ken Ishii, MD, PhD,* Morio Matsumoto, MD, PhD,* Suketaka Momoshima, MD, PhD,‡ Kota Watanabe, MD, PhD,† Takashi Tsuji, MD, PhD,* Hironari Takaishi, MD, PhD,* Masaya Nakamura, MD, PhD,* Yoshiaki Toyama, MD, PhD,* and Kazuhiro Chiba, MD, PhD*

Study Design. A retrospective case series.

Objective. To propose a novel treatment strategy for chronic atlantoaxial rotatory fixation (AARF).

Summary of Background Data. Treatment strategy for chronic or recurrent AARF remains controversial. We have previously reported that a deformity of the superior facet of the axis (C2 facet deformity), which is frequently observed in patients with chronic AARFs, is a risk factor for recurrent dislocation. In this article, we report seven consecutive cases of chronic AARF who underwent closed manipulation followed by external halo fixation and maintained good reduction with the remodeling of the C2 facet deformity.

Methods. Seven girls with a chronic AARF who sustained torticollis for an average of 4.6 months after the onset were referred to our clinic. Closed manipulation by careful manipulation under general anesthesia followed by external immobilization with a halo vest was performed in all cases. Radiographic findings and clinical courses were retrospectively reviewed with approvals by the institutional review board.

Results. Three-dimensional computed tomography images before reduction revealed persistent atlantoaxial subluxation and the C2 facet deformity in the dislocated side in all cases. Follow-up three-dimensional computed tomographic scans demonstrated the remodeling of the C2 facet deformity at an average of 2.8 months after successful reduction of subluxation. Subsequently, the halo vests were removed and gentle neck range of motion exercise was started in all cases. The normal cervical range of motion was obtained 2 weeks after the removal of halo vests in five cases, whereas the range of motion remained limited in two cases. At a mean follow-up of 17.4 months, neither symptoms nor recurrence of subluxation occurred in all cases.

Conclusion. Chronic irreducible and recurrent unstable AARF can be managed successfully by careful closed manipulation followed by halo fixation, if the C1 and C2 have not been osseously fused. The remodeling of the C2 facet deformity detected on follow-up CT scans can be a useful radiographic parameter to determine the appropriate period of halo fixation in this new treatment strategy obviating the need for surgical intervention.

Key words: atlantoaxial rotatory fixation (AARF), chronic subluxation, facet deformity, recurrent subluxation, remodeling.

Spine 2011;36:E256–E262

In 1830, rotatory subluxation of the atlantoaxial joint was reported for the first time by Sir Charles Bell.[1] Persistent subluxation-causing torticollis in children was termed as atlantoaxial rotatory fixation (AARF) by Fielding and Hawkins[2] in 1977. Most acute AARFs can be treated successfully by conservative therapy including closed manipulation or cervical traction followed by a cervical orthosis. On the contrary, in chronic cases, closed reduction and its maintenance is often unsuccessful,[3–10] requiring surgical treatment for patients with chronic irreducible or recurrent unstable AARFs.[2,3,5,6,11–13]

Over the years, improvements in the surgical techniques have brought encouraging treatment results for upper cervical spine pathologies. Posterior C1–C2 arthrodesis has been

From the *Departments of Orthopaedic Surgery, †Advanced Therapy for Spine and Spinal Cord Diseases, and ‡Departments of Radiology, School of Medicine, Keio University, Shinjuku, Tokyo, Japan.

Acknowledgment date: May 8, 2009. Revision date: December 24, 2009. Acceptance date: February 6, 2010.

The article does not contain information about medical device(s)/drug(s).

No funds were received in support of this work. No benefits in any form have been or will be received from a commercial party related directly or indirectly to the subject of this article.

All aspects of this study were approved by Keio University institutional review board and informed consent was obtained from study participant.

Address correspondence and reprint request to Kazuhiro Chiba, MD, PhD, Department of Orthopaedic Surgery, School of Medicine, Keio University, 35 Shinanomachi, Shinjuku, Tokyo 160-8582, Japan; E-mail: kchiba@sc.itc.keio.ac.jp

DOI: 10.1097/BRS.0b013e3181d8bbdd

Copyright © 2011 Lippincott Williams & Wilkins. Unauthorized reproduction of this article is prohibited.

widely used for recurrent unstable AARFs following the closed reduction, and a variety of posterior fusion techniques have been advocated, including posterior wiring methods by Gallie,[14] McGraw and Rusch,[15] and Brooks and Jenkins[16]; transarticular screwing by Magerl[17]; and C1–C2 lateral mass fixation by Goel and Laheri[18] and Harms and Melcher.[19] For irreducible AARF associated with C1–C2 bony union, transoral anterior approach[20,21] and extreme lateral approach[22] have been described as a surgical method for reduction of subluxation before C1–C2 arthrodesis. Therefore, surgical procedures including posterior fixation between C1 and C2 with or without anterior release have been the treatment of choice for cases of chronic irreducible and recurrent unstable AARFs. Although previous reports have demonstrated successful reduction and fixation after surgeries, several complications have also been reported.[23–25] The vertebral artery injury is one of the most serious complications during the C1–C2 transarticular screw and C2 pedicle screw placements.[26,27] After the posterior atlantoaxial fusion, limited neck motion can cause disturbances in activities of daily living.[28,29]

Recent advances in three-dimensional (3D) computed tomography (CT) and magnetic resonance imaging have provided detailed information on the degree and types of subluxation, presence of inflammation, overstretching of the stabilizing ligaments, and primary damages to articular surface in the C1–C2 joint in AARF patients. We have previously reported that a deformity of superior facet of the axis (C2 facet deformity) on 3D CT images observed in chronic AARF cases is a risk factor for the recurrence of AARF.[6] Thereafter, the surgical treatments have routinely been indicated for patients with chronic irreducible or recurrent unstable AARFs in our institute, if the C2 facet deformity was observed on CT. In 2006, the diagnosis of chronic recurrent AARF with the C2 facet deformity was established in an 11-year-old girl who visited our clinic. The surgery was postponed because of unstable physical condition, and she underwent a closed reduction followed by external immobilization using halo vest waiting for the fusion surgery. Surprisingly, the successful remodeling of C2 facet deformity was observed in 3D CT images at the 3-month follow-up. At that time, gentle exercise of neck range of motion (ROM) was started after removal of the halo vest, and the girl regained normal neck ROM without recurrence.

Experience of this case encouraged us to use this remodeling as a radiographic sign to determine the optimal timing for the removal of a halo vest, because we believed that this remodeling process, buttress-like bone formation, can stabilize the atlantoaxial joint, thereby preventing recurrence of subluxation. Since then, seven consecutive patients with a chronic AARF who presented with the C2 facet deformity on 3D CT have been treated successfully by closed manipulation followed by external halo fixation in our institute. The purpose of this study is to describe our new therapeutic strategy for chronic AARF and its clinical outcomes.

MATERIALS AND METHODS

Patients

With the approval of the institutional review board, clinical records of seven consecutive patients with a chronic AARF were retrospectively reviewed. Between October 2006 and September 2008, seven patients who had torticollis for more than 2 months were referred to our hospital, and the diagnoses of chronic AARF were established in all cases. The mean age at the initial visit was 7.3 years (range = 4.3–11.6 years). The mean period between the onset of torticollis and the initial visit to our institute was 4.6 months (range = 2.1–8.8 months), and the mean follow-up duration was 17.4 months (range = 6–28 months). All patients presented with a neck pain, a so-called cock-robin posture, and restricted neck motion, although all of them were neurologically intact. The causes of torticollis were upper respiratory tract infection in four, incidental trauma in one, respiratory tract infection following trauma in one, and unknown in one patient. All patients underwent either halter traction or closed manipulation

TABLE 1. Summary of Clinical Data at the Initial Visit

Case	Type of AARF	Age (yr)	Sex	Cause	Duration of Symptom (mo)	Dislocation Side	ADI (mm)	Fielding Classification	Pang's Type	Our Grade	C2 Facet Deformity	Bony Union
1	Irreducible	11	F	RTI	6.0	Rt	13	3	1	2	++	−
2	Recurrence	8	F	Unknown	3.8	Rt	3.6	2	2	2	+	−
3	Irreducible	7	F	Trauma and RTI	5.4	Rt	7	3	1	3	+++	−
4	Irreducible	4	F	RTI	3.4	Rt	4.2	2	1	3	+	−
5	Irreducible	7	F	Trauma	8.8	Lt	8	3	1	3	+++	−
6	Irreducible	5	F	RTI	2.1	Lt	3.5	1	1	2	+	−
7	Irreducible	5	F	RTI and tympanitis	2.6	Rt	5	2	2	2	+	−

AARF indicates atlantoaxial rotatory fixation; ADI, atlantodental interval; F, female; Lt, left; Rt, right; RTI, upper respiratory tract infection; +, slight; ++, moderate; +++, severe; −, none.

Copyright © 2011 Lippincott Williams & Wilkins. Unauthorized reproduction of this article is prohibited.